Histone deacetylase–mediated regulation of endolysosomal pH

Received for publication, January 21, 2018, and in revised form, March 19, 2018 Published, Papers in Press, March 22, 2018, DOI 10.1074/jbc.RA118.002025

Hari Prasad[1] **and Rajini Rao**[2]

From the Department of Physiology, The Johns Hopkins University School of Medicine, Baltimore, Maryland 21205

Edited by John M. Denu

The pH of the endolysosomal system is tightly regulated by a balance of proton pump and leak mechanisms that are critical for storage, recycling, turnover, and signaling functions in the cell. Dysregulation of endolysosomal pH has been linked to aging, amyloidogenesis, synaptic dysfunction, and various neurodegenerative disorders, including Alzheimer's disease. Therefore, understanding the mechanisms that regulate luminal pH may be key to identifying new targets for managing these disorders. Meta-analysis of yeast microarray databases revealed that nutrient-limiting conditions inhibited the histone deacetylase (HDAC) Rpd3 and thereby up-regulated transcription of the endosomal Na^+/H^+ exchanger Nhx1, resulting in vacuolar alkalinization. Consistent with these findings, Rpd3 inhibition by the HDAC inhibitor and antifungal drug trichostatin A induced Nhx1 expression and vacuolar alkalinization. Bioinformatics analysis of *Drosophila* and mouse databases revealed that caloric control of the Nhx1 orthologs DmNHE3 and NHE6, respectively, is also mediated by HDACs. We show that NHE6 is a target of the transcription factor cAMP-response element–binding protein (CREB), a known regulator of cellular responses to low-nutrient conditions, providing a molecular mechanism for nutrient- and HDAC-dependent regulation of endosomal pH. Of note, pharmacological targeting of the CREB pathway to increase NHE6 expression helped regulate endosomal pH and correct defective clearance of amyloid Aβ in an apoE4 astrocyte model of Alzheimer's disease. These observations from yeast, fly, mouse, and cell culture models point to an evolutionarily conserved mechanism for HDAC-mediated regulation of endosomal NHE expression. Our insights offer new therapeutic strategies for modulation of endolysosomal pH in fungal infection and human disease.

The endosome is a busy way station that handles cargo traffic at the cross-roads of degradation and recycling. An important hallmark of the endolysosomal system is a pH gradient that is increasingly acidic through the transition from early, recycling, and late endosomes to the lysosome (1). Precise tempo-spatial pH_{lumen} regulation within each of these specialized compartments is critical for a range of functions, including controlling cargo sorting, vesicular budding and formation of intraluminal vesicles, dissociation of internalized ligands, receptor recycling and turnover, modulating enzyme activity, antigen processing, and cellular signaling (2).

Endosomes are acidified by the electrogenic pumping of protons by the V-type H^+-ATPase in conjunction with vesicular chloride transporters of the CLC family that shunt the membrane potential, effectively allowing a build-up of luminal protons (3, 4). Proton leak mechanisms consisting of proton conduction channels or proton-coupled antiporters limit the acidification, and the balance of pump and leak pathways defines the pH set point. Although the molecular identity of vesicular proton channels remains poorly defined, more recently, endosomal Na^+/H^+ exchangers (eNHE)[3] have emerged as the dominant leak pathway for luminal protons. Because exchanger mechanisms have high transport rates of ~1,500 ions/s (5), they overwhelm the capacity of the proton pump so that even small changes in eNHE activity or expression result in significant pH changes within the endolysosomal system.

The fundamental importance of endosomal pH is highlighted by the fact that a growing number of human diseases are associated with mutations in V-ATPase subunits (*e.g.* osteopetrosis, renal tubular acidosis, cutis laxa), chloride transporters (*e.g.* Dent's disease), and eNHE (Christianson syndrome, autism, and attention deficit hyperactivity disorder) (3, 4, 6). Furthermore, defective endolysosomal pH regulation is being increasingly linked to cellular aging, amyloidogenesis, synaptic dysfunction, and neurodegenerative disorders, including Alzheimer's disease (7, 8). Therefore, the discovery of novel regulators of endolysosomal pH may be crucial to identifying new diagnostic and therapeutic targets for these disorders.

As a starting point, we turned to the yeast *Saccharomyces cerevisiae*, which has powerfully informed our understanding of fundamental mechanisms of endocytosis and vesicular traffic that are functionally conserved with higher organisms (9). By

This work was supported by the Johns Hopkins Medicine Discovery Fund (to R. R.). This work was also supported by National Institutes of Health Grant DK054214 (to R. R.). The authors declare that they have no conflicts of interest with the contents of this article. The content is solely the responsibility of the authors and does not necessarily represent the official views of the National Institutes of Health.

This article contains Figs. S1–S8.

[1] A Fulbright Fellow supported by the International Fulbright Science and Technology Award.

[2] To whom correspondence should be addressed: Dept. of Physiology, The Johns Hopkins University School of Medicine, Baltimore, MD 21205. Tel.: 410-955-4732; E-mail: rrao@jhmi.edu.

[3] The abbreviations used are: eNHE, endosomal Na^+/H^+ exchanger(s); HDAC, histone deacetylase; CRE, cAMP-response element; CREB, CRE-binding protein; FDA, Food and Drug Administration; TSA, trichostatin A; BDNF, brain-derived neurotrophic factor; kb, kilobase(s); TSS, transcription start site; AD, Alzheimer's disease; DMEM, Dulbecco's modified Eagle's medium; qPCR, quantitative PCR; SV40, simian virus 40; CTX, cortex.

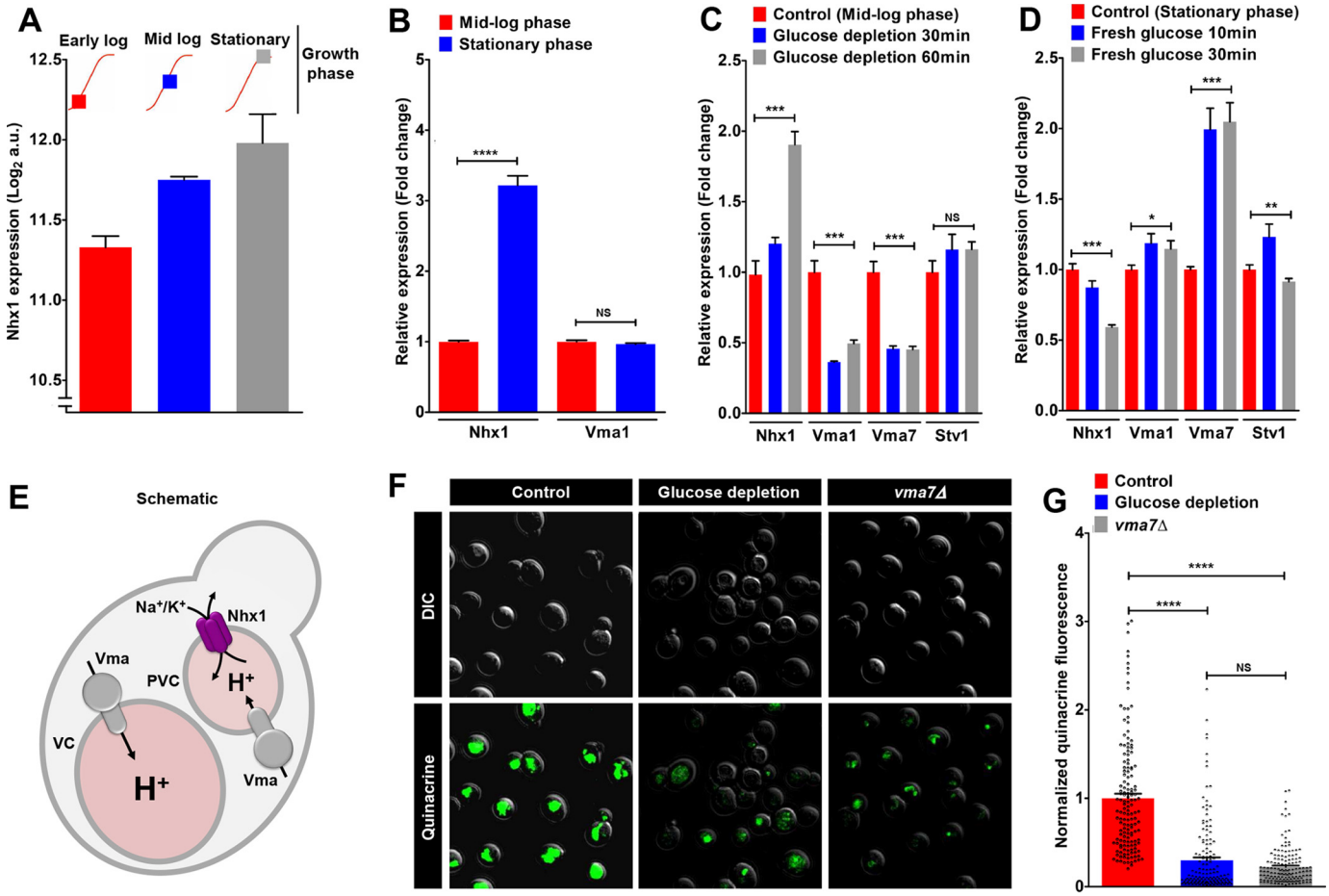

Figure 1. Nutrient control of endolysosomal pH in yeast. *A*, microarray data analysis revealed increasing expression of Nhx1 with growth, sampled as indicated in the growth-phase representation. Note that maximal expression was in stationary phase, which is associated with glucose/nitrogen limitation). *B*, qPCR validation of Nhx1 expression showed 3.2-fold up-regulation of Nhx1 transcript in stationary-phase yeast, compared with mid-log phase (****, $p < 0.0001$; $n = 3$; Student's *t* test). No change in V-ATPase subunit Vma1 levels was observed ($p = 0.092$; Student's *t* test). *C*, glucose removal from mid-log–phase yeast cultures showed a ~2-fold increase in Nhx1 mRNA within 60 min of depletion (***, $p < 0.001$; $n = 3$; Student's *t* test). Note significant down-regulation of V-ATPase subunits with acute glucose depletion (***, $p < 0.001$, Vma1; ***, $p < 0.001$, Vma7). *D*, conversely, the addition of glucose (2%) to stationary-phase cultures showed significant decrease in Nhx1 mRNA within 30 min (***, $p < 0.001$; $n = 3$; Student's *t* test). Note significant up-regulation of V-ATPase subunits with glucose addition (*, $p < 0.05$, Vma1; ***, $p < 0.001$, Vma7). *C* and *D*, in contrast to Vma1 and Vma7, secretory pathway isoform Stv1 expression showed modest or no changes in response to glucose, suggesting that the effect of glucose regulation on the V-ATPase is largely localized to endosomal/vacuolar compartments. *E*, schematic to show that Nhx1 functions as a leak pathway for protons within the endosomal/prevacuolar compartment, to balance the proton pump activity of the V-ATPase (*Vma*). *F* and *G*, representative micrographs (*F*) and quantification (*G*) showing loss of quinacrine fluorescence with acute glucose depletion, similar to V-ATPase– deficient *vma7*Δ mutants, pointing to increased vacuolar alkalization (****, $p < 0.0001$; $n = 100$; Student's *t* test). *NS*, not significant. *Error bars*, S.D.

leveraging data from yeast to fly and mammalian models, we discovered an evolutionarily conserved mechanism for epigenetic control of eNHE by histone deacetylases (HDACs) in response to nutrient availability. In mammalian cells, HDAC-mediated control of endolysosomal pH occurs by transcriptional regulation of the endosomal Na^+/H^+ exchanger NHE6 (*SLC9A6*) via the cAMP-response element– binding protein (CREB) pathway. We show that elevation of cAMP levels by the FDA-approved drug Rolipram results in CREB activation, increased NHE6 expression, and restoration of defective Aβ clearance in the apoE4 astrocyte model of late onset Alzheimer's disease.

Histone acetylation has been widely recognized as a key modulator of global chromatin structure that dynamically couples extracellular signals to gene transcription. Whereas lysine acetylation on histone tails interferes with generation of higher-order chromatin structures and promotes access and binding of transcription factors, histone deacetylation favors chromatin packing and represses gene transcription (10–12). HDAC inhibitors have been approved for the treatment of hematologic cancers and are being considered as a promising therapy to reverse disease-associated epigenetic states in a range of cardiovascular, neurodegenerative, and inflammatory diseases (11–14). Given their broad application, our findings offer potential therapeutic options to treat endolysosomal pH dysfunction in autism, AD, and other neurodegenerative disorders.

Results

Nutrient control of endolysosomal pH in yeast

Yeast microarray data sets are a valuable resource for discovery-driven mining efforts. A meta-analysis of 45 microarray experiments that included 937 samples revealed increasing expression of Nhx1, with growth phase stationary > mid-log >

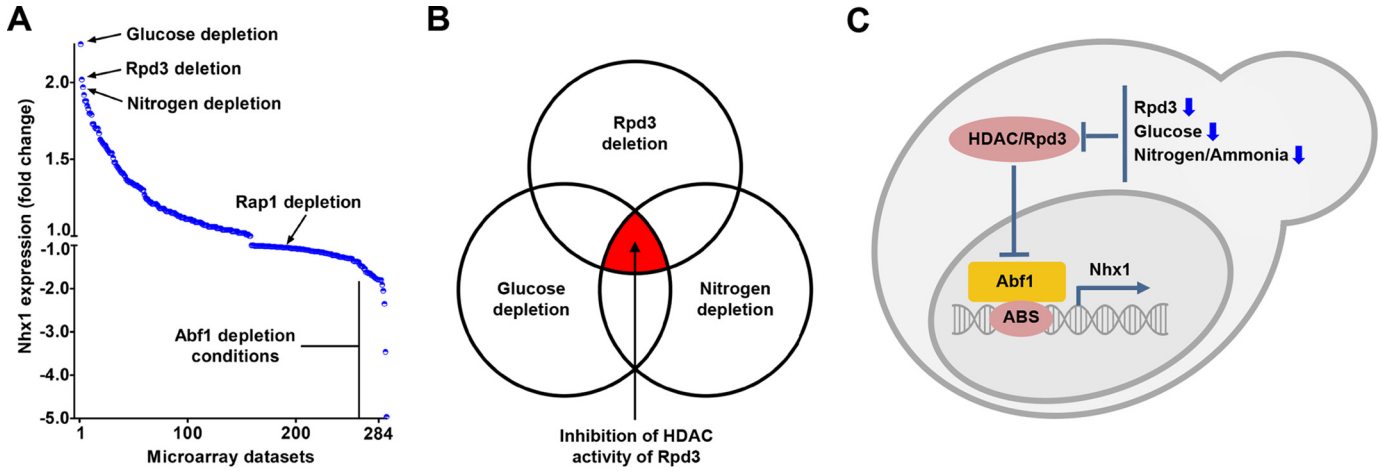

Figure 2. Discovery of the Rpd3-Abf1 axis for regulation of Nhx1 expression by histone deacetylases. *A*, waterfall plot depicting -fold change in Nhx1 expression (*y* axis) obtained from an unbiased bioinformatics analysis of 284 microarray studies (*x* axis), as described under "Experimental procedures." Note that all five conditions leading to maximal down-regulation of Nhx1 were linked to depletion of Abf1 transcription factor, known to be negatively regulated by Rpd3. *B*, HDAC activity of Rpd3 was common to all three microarray experiments that gave maximal up-regulation of Nhx1 expression, namely (i) genetic deletion of Rpd3, (ii) glucose depletion, and (iii) nitrogen depletion. *C*, HDAC–Rpd3-Abf1-Nhx1 axis for regulation of Nhx1 expression. This model predicts that inhibition of Rpd3 activity releases the brake on Abf1, which in turn binds to the Abf1-binding site (*ABS*) on the Nhx1 promoter and enhances its expression. See related Fig. S1.

early log (Fig. 1*A*), which we independently confirmed; Nhx1 transcript increased by 3.2-fold in stationary-phase cells, compared with mid-log phase (Fig. 1*B*). Stationary-phase growth in yeast is associated with depletion of nutrients. To determine whether growth-phase regulation of Nhx1 was linked to glucose availability, we tested the effect of glucose removal from mid-log phase yeast cultures. Nhx1 mRNA was increased by nearly 2-fold within 60 min of glucose removal ($p < 0.001$; Fig. 1*C*). In contrast, the addition of glucose (2%) to stationary-phase cultures elicited significant decrease in Nhx1 mRNA within 30 min ($p < 0.001$; Fig. 1*D*).

Nhx1 functions as a leak pathway for protons within the endosome/prevacuolar compartment, in opposition to the proton pump activity of the V-ATPase (15) (Fig. 1*E*). The balance of proton pump and leak sets the pH within the endolysosomal compartments. Therefore, we also analyzed expression of V-ATPase subunits under the same experimental conditions. Although we did not observe a growth phase– dependent transcriptional change in the V-ATPase catalytic subunit Vma1 (Fig. 1*B*), V-ATPase subunits were significantly down-regulated with acute glucose depletion ($p < 0.001$, Vma1; $p < 0.001$, Vma7; Fig. 1*C*) and up-regulated upon glucose addition ($p < 0.05$, Vma1; $p < 0.001$, Vma7; Fig. 1*D*) in contrast to Nhx1. Previous studies have shown that yeast V-ATPase subunit Stv1 is selectively targeted to the Golgi/secretory pathway and is not required for vacuolar acidification and function (16, 17). In contrast to Vma1 and Vma7, Stv1 expression showed modest or no changes in response to glucose (Fig. 1, *C* and *D*), suggesting that the effect of glucose regulation on the V-ATPase is largely localized to late endosomal/vacuolar compartments.

We predicted that reciprocal transcriptional changes in Nhx1 and V-ATPase subunits would alter the pH of the yeast vacuole. Vacuolar pH can be probed *in situ* with the pH-sensitive fluorescent dye quinacrine, which accumulates in acidic environments (18). Following glucose depletion, yeast vacuoles showed little or no quinacrine staining, similar to V-ATPase–deficient *vma7*Δ mutants (Fig. 1, *F* and *G*; $p < 0.0001$, $n = 100$). Consistent with the potential role for Nhx1 in regulating nutrient control of endolysosomal pH in yeast, *nhx1*Δ mutants showed severely reduced survival during the stationary-phase growth (19). Post-translational regulation of V-ATPase disassembly and reassembly in response to glucose concentration is well established (20, 21). Here, we conclude that glucose also elicits reciprocal transcriptional changes in proton pump and leak mechanisms to regulate the pH gradient across yeast vacuoles.

Regulation of endolysosomal pH in yeast is mediated by a histone deacetylase

We extended our unbiased bioinformatics approach to analyze data from 284 microarray studies that comprised a wide range of experimental conditions, including gene deletion, overexpression, and mutations; drug/toxin treatment; nutrient limitation or excess; metabolic/environmental stress; and more. We identified experimental conditions eliciting a minimum of ±2-fold change in *NHX1* gene expression (Fig. 2*A* and Fig. S1*A*). The highest up-regulation of Nhx1 was observed under conditions of (i) genetic deletion of Rpd3, (ii) glucose depletion, and (iii) nitrogen depletion. Pathway analysis revealed that loss or inhibition of HDAC activity of Rpd3 was common to all three of these conditions (22, 23) (Fig. 2*B*). Thus, nutrient (glucose or nitrogen) depletion preserves histone acetylation by replacement and inactivation of the HDAC-Rpd3 complex from the promoters of specific genes (22). Consistent with this finding, Rpd3 deletion phenocopies calorie restriction by enhancing lifespan of yeast cells (24, 25). Conversely, all five conditions leading to maximal down-regulation of Nhx1 were linked to depletion of Abf1, an essential transcription factor that is negatively regulated by Rpd3 (26–28) (Fig. 2*A* and Fig. S1*A*). Recent evidence suggests that Abf1 is activated during nutritional stress (29). Furthermore, Abf1 is predicted to bind to the *NHX1* promoter (Fig. S1*B*), and chromatin immu-

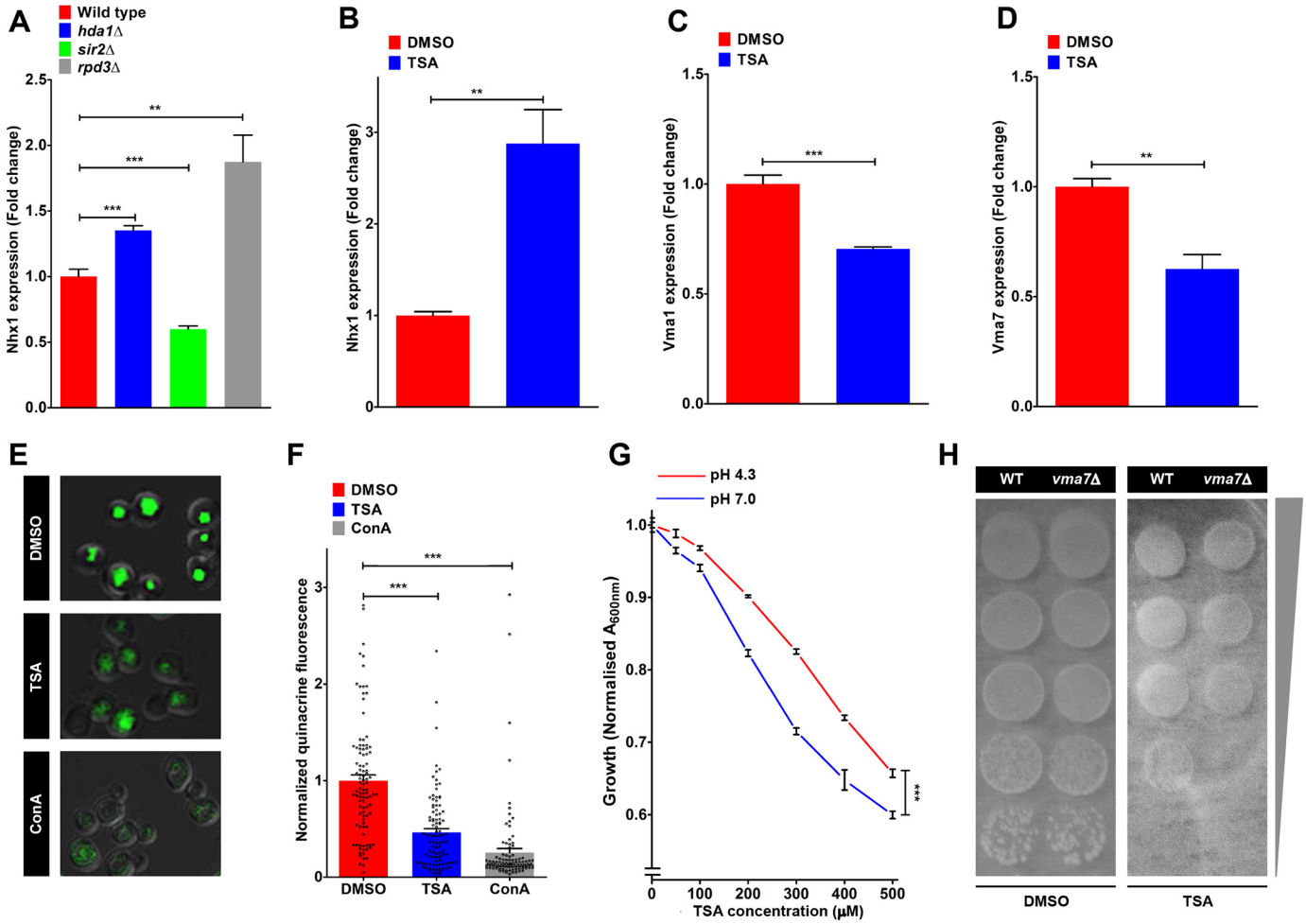

Figure 3. Regulation of endolysosomal pH in yeast is mediated by a histone deacetylase. *A*, deletion of Rpd3 (*rpd3*Δ strain) increased *NHX1* transcript by 1.9-fold relative to isogenic WT yeast (**, $p = 0.002$; $n = 3$; Student's *t* test). Deletion of two other histone deacetylase genes led to lesser *NHX1* induction (1.35-fold in *hda1*Δ; ***, $p = 0.0008$; $n = 3$; Student's *t* test) or repression (0.6-fold in *sir2*Δ; ***, $p = 0.0003$; $n = 3$; Student's *t* test). *B*, TSA treatment of WT yeast elicited significant 2.88-fold up-regulation of Nhx1 transcript (**, $p = 0.001$; $n = 3$; Student's *t* test) mimicking the effect of Rpd3 deletion. *C* and *D*, qPCR analysis of V-ATPase subunits showed significant down-regulation of Vma1 (~30% lower; ***, $p = 0.0003$; $n = 3$; Student's *t* test) (*C*) and Vma7 (~37% lower; **, $p = 0.001$; $n = 3$; Student's *t* test) (*D*) in TSA-treated yeast, compared with vehicle treatment. *E* and *F*, representative micrographs (*E*) and quantification (*F*) showing loss of quinacrine fluorescence with TSA treatment, similar to treatment with a V-ATPase inhibitor concanamycin A (*ConA*), pointing to increased vacuolar alkalization (***, $p < 0.0001$; $n = 100$; Student's *t* test). *G*, alkaline pH sensitivity is a defining phenotype of increased vacuolar pH. TSA-treated cells show dose-dependent reduction of growth at medium pH of 7.0 as compared with pH of 4.3 (***, $p < 0.001$; $n = 4$; Student's *t* test). *H*, a spotting assay on YPD agar plates was performed to demonstrate hypersensitivity to TSA in the *vma7*Δ yeast, lacking V-ATPase activity, indicative of synthetic lethality. See related Fig. S2. *Error bars*, S.D.

noprecipitation with DNA microarray (ChIP-on-chip) data from the Saccharomyces Genome Database (SGD) provided experimental evidence for Abf1 binding to the *NHX1* promoter (30). For comparison, depletion of another general regulatory transcription factor, Rap1, had no effect on Nhx1 expression (Fig. 2*A* and Fig. S1*A*). Although more direct studies are needed to confirm Rpd3-Abf1 occupancy of the *NHX1* promoter, bioinformatics analysis of all top hits in *NHX1* gene expression (both up- and down-regulation) funneled into a single pathway: the Rpd3-Abf1-Nhx1 axis (Fig. 2*C*).

To confirm and extend these *in silico* observations, we independently demonstrated that Nhx1 transcript was elevated by 1.9-fold in the *rpd3*Δ mutant, relative to isogenic WT yeast (Fig. 3*A*). Other histone deacetylase gene deletions conferred more modest induction (1.35-fold in *hda1*Δ; Fig. 3*A*) or repression (0.6-fold in *sir2*Δ; Fig. 3*A*). All three yeast deletion strains showed similar growth (Fig. S2*A*). Restoration of Rpd3 by ectopic expression under a galactose-inducible promoter in *rpd3*Δ not only abolished Nhx1 up-regulation in stationary phase, but also caused further repression (68% lower) in mid-logarithmic cells and inhibited yeast growth (Fig. S2, *B* and *C*).

Yeast Rpd3 is a target of the histone deacetylase inhibitor and fungal antibiotic trichostatin A (TSA), and the transcriptional profile of TSA-treated WT yeast is similar to that of *rpd3*Δ yeast (23). We show that that TSA treatment of WT yeast elicited significant 2.9-fold up-regulation of Nhx1 transcript (Fig. 3*B*), mimicking the effect of Rpd3 deletion. In contrast, we observed significant down-regulation of V-ATPase subunits Vma1 (~30% lower; Fig. 3*C*) and Vma7 (~37% lower; Fig. 3*D*) in TSA-treated yeast, compared with vehicle treatment. In contrast to Vma1 and Vma7, the levels of Stv1 did not change significantly with TSA treatment (Fig. S2*D*), suggesting that the effect of TSA is specific to V-ATPase localized to the vacuolar compartment.

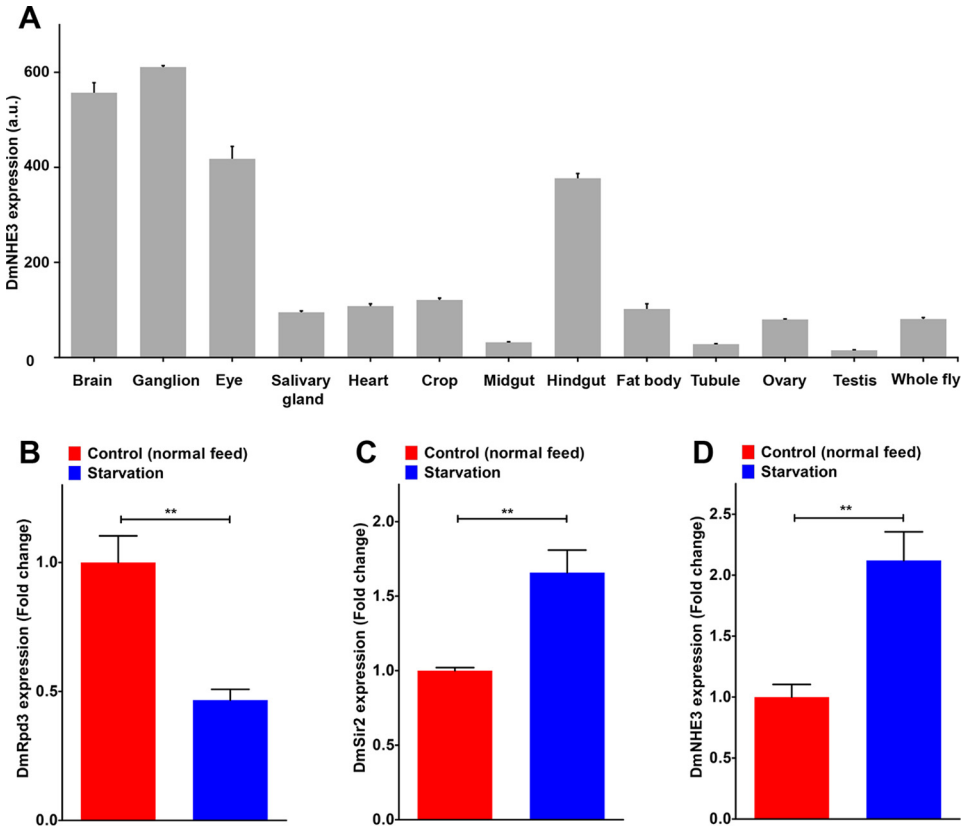

Figure 4. Evolutionary conservation of eNHE regulation by nutrient availability and histone deacetylases. *A*, expression pattern of *Drosophila* eNHE isoform DmNHE3. Note the high expression of DmNHE3 in the brain, like its mammalian cousin NHE6. Data were obtained from the FlyBase atlas. *a. u.*, arbitrary units. *B* and *C*, gene expression data showing significant down-regulation of class I HDAC DmRpd3 (−2.14-fold; **, $p = 0.0012$; $n = 3$; Student's *t* test; *B*) and reciprocal up-regulation of class III HDAC DmSir2 (1.66-fold; **, $p = 0.0017$; $n = 3$; Student's *t* test; *C*) in fly larvae starved for 24 h. *D*, significant up-regulation (2.12-fold; **, $p = 0.0017$; $n = 3$; Student's *t* test) of DmNHE3 expression with starvation suggests an evolutionarily conserved mechanism for regulation of eNHE expression by histone deacetylases in yeast and fly models. See related Fig. S3. *Error bars*, S.D.

The transcriptional up-regulation of Nhx1 and concomitant down-regulation of vacuolar V-ATPase subunits by TSA is predicted to alkalinize the yeast vacuole (3). Compared with robust quinacrine fluorescence in WT yeast vacuoles (18), TSA treatment drastically reduced vacuolar accumulation of quinacrine, similar to the effect of the well-characterized V-ATPase inhibitor concanamycin A, pointing to increased vacuolar pH (Fig. 3, *E* and *F*). Alkaline pH sensitivity is a defining phenotype of V-ATPase mutants, indicative of the reduced ability to acidify vacuoles (31, 32). We found that TSA-treated cells show dose-dependent reduction of growth at alkaline medium pH (Fig. 3*G*). Hypersensitivity to TSA in the *vma7*Δ yeast, lacking V-ATPase activity, is evidenced by synthetic lethality (Fig. 3*H* and Fig. S2*E*). TSA synergizes with the antifungal action of an azole drug fluconazole that we previously showed to act via inhibition of V-ATPase activity (31)(Fig. S2*F*). Together, these data provide strong evidence for regulation of yeast vacuolar pH by HDAC inhibition.

Evolutionary conservation of eNHE regulation by nutrient availability and histone deacetylases

To investigate whether the mechanism of up-regulation of eNHE in response to nutrient limitation and HDAC activity is evolutionarily conserved, we evaluated publicly available expression data in the fruit fly *Drosophila melanogaster*. Fruit fly has one eNHE isoform, DmNHE3, which, like its mammalian cousin NHE6, is highly expressed in the brain (33) (Fig. 4*A*). Analysis of a microarray data set studying the effects of starvation in *Drosophila* larvae (GSE14531) revealed significant down-regulation of class I HDAC DmRpd3 (−2.14-fold; Fig. 4*B*) and reciprocal up-regulation of class III HDAC DmSir2 (1.66-fold; Fig. 4*C*) in fly larvae starved for 24 h (34). Importantly, consistent with findings from yeast, there was significant up-regulation (2.12-fold; Fig. 4*D*) of DmNHE3 expression with starvation (34). No changes in expression with starvation were seen for other NHE isoforms, DmNHE1 and DmNHE2 (Fig. S3, *A* and *B*). We also evaluated the effect of nutrient depletion on transcript levels of Vha68 and Vha14, which are orthologs of Vma1 and Vma7, respectively. Unlike our observations in yeast, no change in expression of these V-ATPase subunits was noted in *Drosophila*, suggesting that the transcriptional effect of starvation might be limited to endosomal NHE in higher eukaryotes.

Chromatin-modifying complexes are conserved between yeast and mammals. Eighteen mammalian HDACs have been described, grouped into four functional classes based on similarity to yeast orthologs (10). Independent studies have shown that insulin, the principal hormone orchestrating response to glucose availability, alters HDAC nuclear translocation in mammalian cells (35). Calorie restriction has been shown to improve insulin sensitivity and mimic the effects caused by

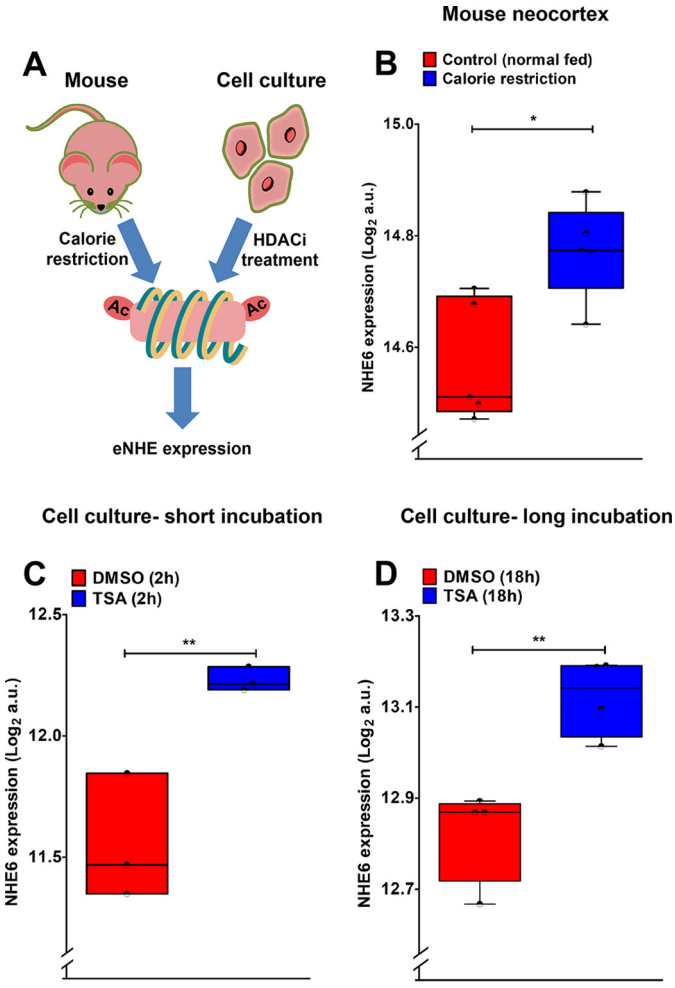

Figure 5. Calorie restriction and HDAC inhibition increase NHE6 expression. *A*, schematic to show that dietary calorie restriction mimics the effects caused by HDAC inhibitors (*HDACi*) and predicted to alter eNHE expression. *B*, calorie restriction (~10% lower than *ad libitum* intake) in the mouse significantly increased NHE6 expression in the neocortex (*, $p = 0.01$; $n = 5$; Student's *t* test). *a. u.*, arbitrary units. *C* and *D*, gene expression data from two independent microarray experiments studying the effect of TSA in cell culture at shorter (2-h) and longer (18-h) time points. TSA treatment significantly increased NHE6 expression ($p = 0.011$; *, $n = 3$; Student's *t* test; 2 h; *C*) (**, $p = 0.0046$; $n = 4$; Student's *t* test; 18 h; *D*) at both time points. See related Figs. S4 and S5.

HDAC inhibitors, including on histone acetylation and activation of CREB (36–39). Intriguingly, the mammalian eNHE ortholog NHE6 is a reported insulin-responsive protein, and its subcellular trafficking is regulated by insulin (40). Furthermore, in neurons, loss of NHE6 has been reported to attenuate brain-derived neurotrophic factor (BDNF) signaling that is downstream of insulin and the CREB cascade (41, 42). Given that Na^+/H^+ exchangers are estimated to have very high transport rates of ~1,500 ions/s (5), even small changes in expression may be functionally significant. Therefore, to test whether calorie restriction or HDAC inhibitors enhance mammalian eNHE expression, we first analyzed publicly available expression data on caloric restriction (~10% lower than *ad lib* intake) in the mouse (Fig. 5*A*). These data revealed significant up-regulation of NHE6 in the neocortex (Fig. 5*B*) but not of the closely related endosomal NHE9 or V-ATPase subunit Vma1/ATP6V1A (Fig. S4, *A* and *B*) (43). Next, we analyzed two independent microarray experiments studying the effect of TSA in cell culture at shorter (2 h; GSE8488) and longer (18 h; GSE9247) time points (44, 45). Expression data from both of these experiments revealed significant up-regulation of NHE6 with TSA treatment (Fig. 5, *C* and *D*), but not NHE9 (Fig. S5, *A–D*) or NHE1 (Fig. S5, *B–E*). Activation of transcription factor CREB is a common response to both calorie restriction and pharmacological HDAC inhibition (12, 39). Thus, for comparison, we evaluated a prototypic CREB target BDNF and documented significant up-regulation with calorie restriction in mice (Fig. S4*C*) and HDAC inhibition in cell culture (Fig. S5, *C–F*), as predicted. These observations from yeast, fly, mouse, and cell culture models support our hypothesis of an evolutionarily conserved mechanism for regulation of eNHE expression by histone deacetylases.

NHE6 is a transcriptional target of CREB

Next, we attempted to identify the HDAC-regulated transcription factor equivalent to yeast Abf1 in higher eukaryotes. In the absence of direct Abf1 orthologs in the *Drosophila* or human genome, we looked for parallel starvation response pathways between human and yeast. Various studies suggest that CREB transcription factor regulates the response to nutrient deprivation and glucose availability in mammalian cells, analogous to the Abf1 transcription factor in yeast (39, 46). Both class I (HDAC1) and class II (HDAC4) HDACs directly interact with CREB and negatively regulate its function (47, 48). Furthermore, similar to the Abf1 transcription factor in yeast, the phosphorylation state of CREB is tightly regulated in response to nutrient and glucose availability (39, 49). Based on all of these observations, we hypothesized NHE6 as a potential CREB target (Fig. 6*A*).

Analysis of a publicly available data set of CREB target genes, from ChIP with DNA microarray (ChIP-on-chip) (50), using the recommended cutoff for ChIP-positive genes (binding ratio ≥1.5 and $\log_{10} p$ value ≥3) revealed NHE6 as a potential CREB target. The ChIP binding data for NHE6 were similar to those of DUSP1, a known CREB target, whereas no CREB occupancy was detected for the related NHE7 isoform (Fig. 6, *B* and *C*). Consistent with our hypothesis in Fig. 6*A*, TSA treatment resulted in a ~5.2-fold increase in NHE6 expression in HEK293 cells (Fig. 6*D*), whereas, modest increases were observed in NHE7 (~1.3-fold; Fig. S6*A*) and NHE9 (~1.4-fold; Fig. 6*D*), and no changes in expression of V-ATPase subunits V0a1 (lysosomal) and V0a2 (putative endosomal) were observed (Fig. S6, *B* and *C*). We used the firefly and *Renilla* luciferase reporter gene system to demonstrate significant activation of cAMP-response element (CRE) with TSA treatment (10 μM, 12 h), relative to vehicle control ($p = 0.0064$; Fig. 6, *D* and *E*). To establish a causal link between CREB activation and NHE6 expression, we treated HEK293 cells with forskolin, an adenylyl cyclase activator, and confirmed a significant increase in NHE6 transcript levels that was blocked by expression of a constitutively active/nuclear HDAC4 mutant (S246A/S467A/S632A) (Fig. 6*G*).

To directly test whether NHE6 is a CREB target, we expressed FLAG-tagged CREB1 plasmid in HEK293 cells and assessed (i) functional expression of NHE6 and (ii) binding of

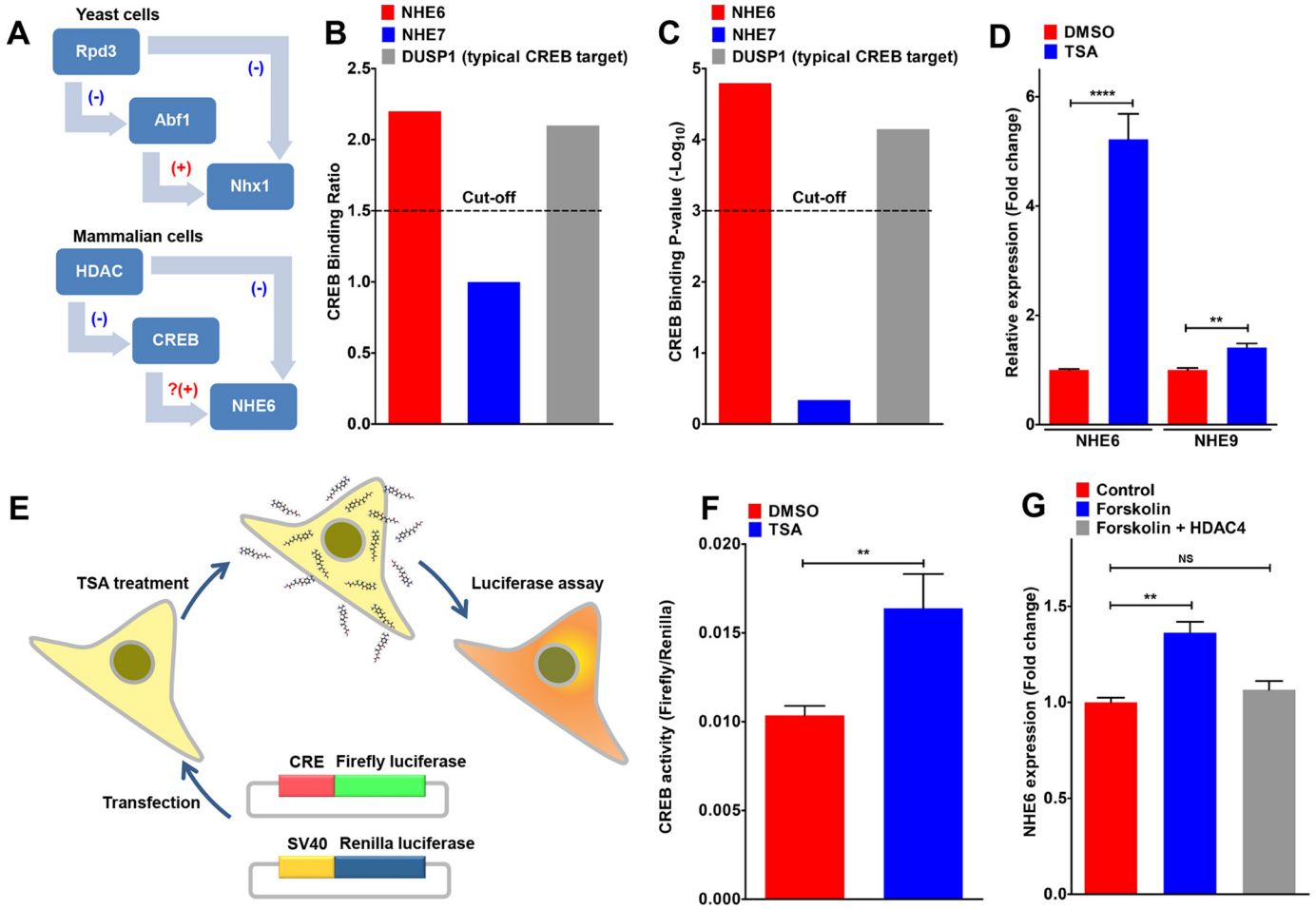

Figure 6. Regulation of NHE6 expression is mediated by a histone deacetylase. *A*, schematic to draw parallels between regulation of eNHE in yeast (*top*) and mammalian cells (*bottom*). CREB transcription factor regulates response to nutrient deprivation and glucose availability in mammalian cells, analogous to the Abf1 transcription factor in yeast. Both class I (HDAC1) and class II (HDAC4) HDACs directly interact with CREB and negatively regulate its function. Based on this predictive model, we hypothesized NHE6 as a potential CREB target. *B* and *C*, ChIP-on-chip (ChIP with DNA microarray) data analyzed using the recommended cutoff for ChIP-positive genes (binding ratio ≥1.5 and $\log_{10}$ *p* value ≥3) revealed NHE6 as a potential CREB target. Note that the ChIP binding data for NHE6 were similar to those of DUSP1, a known CREB target, whereas no CREB occupancy was detected for the related NHE7 isoform. *D*, qPCR analysis demonstrating prominent ~5.2-fold increase in NHE6 expression (****, $p < 0.0001$; $n = 3$; Student's *t* test) and modest increases in NHE9 (~1.4-fold; **, $p = 0.0011$; $n = 3$; Student's *t* test) with TSA treatment of HEK293 cells. *E* and *F*, luciferase assay to confirm TSA-induced activation of CREB using a CRE that drives a firefly luciferase reporter gene and is measured luminometrically (*E*). *Renilla* luciferase driven by a constitutively active SV40 promoter was used to normalize for variation of cell number and transfection efficiency. Significant activation of the CRE was seen with TSA treatment (10 μM; 12 h; *F*) in HEK293 cells, relative to vehicle control (**, $p = 0.0064$; $n = 3$; Student's *t* test). *G*, qPCR analysis to determine the potential of forskolin to augment the expression of NHE6 in HEK293 cells. Note the significant increase in NHE6 transcript levels with forskolin treatment (***, $p = 0.0005$; $n = 3$; Student's *t* test), which was blocked by expression of a constitutively active/nuclear HDAC4 mutant (S246A/S467A/S632A) ($p = 0.116$; $n = 3$; Student's *t* test). *NS*, not significant. See related Fig. S6. *Error bars*, S.D.

CREB to the NHE6 promoter by ChIP-qPCR (Fig. 7*A*). Expression of CREB1 in HEK293 cells significantly elevated NHE6 transcript (Fig. 7*B*), resulting in alkalization of endosomal pH from 5.9 ± 0.03 to 6.12 ± 0.05 (Fig. 7*C*). In contrast, no changes in NHE6 transcript or endosomal pH were observed with the nonphosphorylatable mutant of CREB1 (S133A; Fig. 7, *B* and *C*). ChIP was performed with a ChIP grade anti-FLAG mouse antibody (Fig. 7*D*). Using real-time qPCR, we amplified three predicted CREB binding sites in the promoter of NHE6 (*SLC9A6*) at positions −12, +1, and +2 kb relative to the transcription start site (TSS) (Fig. 7*D* and Fig. S6*D*). For comparison, we used primers targeted to the NHE9 (*SLC9A9*) promoter at position −1 kb relative to TSS (Fig. 7*E*). We confirmed CREB binding to NHE6 promoter at all three predicted sites (Fig. 7, *F–H*). In contrast, we observed no significant binding of CREB to the NHE9 promoter (Fig. 7*I*). Specific pulldown of CREB1 was confirmed by probing the ChIP samples with an antibody against CREB raised in rabbits (Fig. 7*J*). Consistent with our ChIP-qPCR findings, we note that the pattern of NHE6 expression closely parallels that of CREB1 through normal human brain development (Fig. S7*K*; Pearson correlation, 0.62) and in all areas of the brain (Fig. 7*L*). In contrast, NHE9 expression showed no correlation with CREB (Fig. 7*M*; Pearson correlation, −0.018). Taken together, our findings reveal a novel mechanism of CRE-mediated transcriptional regulation of NHE6 and provide a molecular mechanism for nutrient- and HDAC-dependent regulation of endosomal pH.

Control of NHE6 expression by pharmacological targeting of CREB pathway

Christianson syndrome patients, with loss of function mutations in NHE6, clinically present with neurodevelopmental disorders of intellectual disability and severe autism and show age-dependent hallmarks of neurodegeneration, including loss of

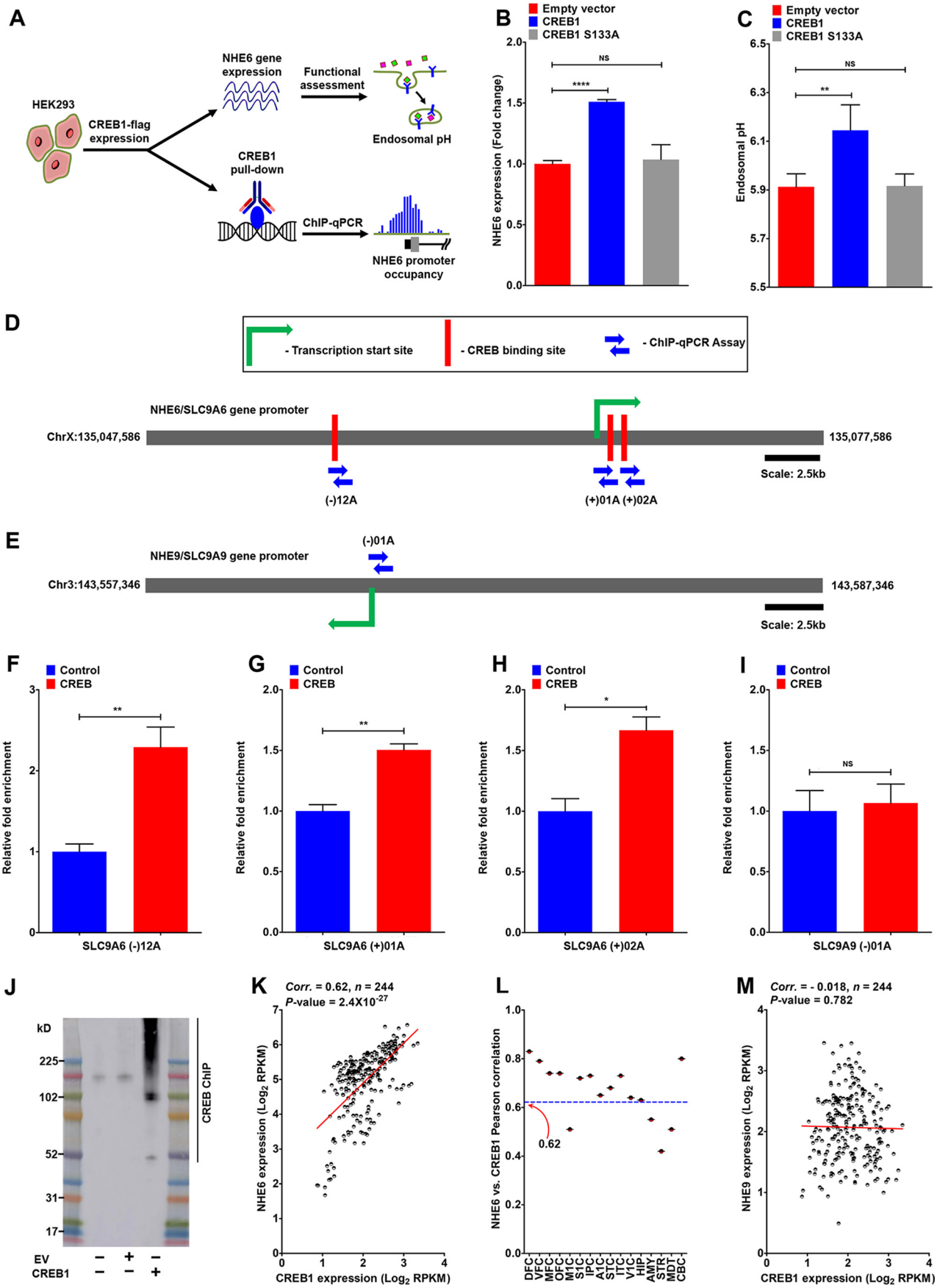
A
HEK293
CREB1-flag expression
NHE6 gene expression
Functional assessment
Endosomal pH
CREB1 pull-down
ChIP-qPCR
NHE6 promoter occupancy
B
Empty vector
CREB1
CREB1 S133A
NHE6 expression (Fold change)
NS
****
C
Empty vector
CREB1
CREB1 S133A
Endosomal pH
NS
**
D
- Transcription start site
- CREB binding site
- ChIP-qPCR Assay
NHE6/SLC9A6 gene promoter
ChrX:135,047,586
135,077,586
Scale: 2.5kb
(-)12A
(+)01A (+)02A
E
NHE9/SLC9A9 gene promoter
(-)01A
Chr3:143,557,346
143,587,346
Scale: 2.5kb
F
Control
CREB
Relative fold enrichment
**
SLC9A6 (-)12A
G
Control
CREB
Relative fold enrichment
**
SLC9A6 (+)01A
H
Control
CREB
Relative fold enrichment
*
SLC9A6 (+)02A
I
Control
CREB
Relative fold enrichment
NS
SLC9A9 (-)01A
J
kD
225
102
52
31
17
CREB ChIP
EV
CREB1
K
Corr. = 0.62, n = 244
P-value = 2.4X10-27
NHE6 expression (Log2 RPKM)
CREB1 expression (Log2 RPKM)
L
NHE6 vs. CREB1 Pearson correlation
0.62
DFC VFC MFC OFC M1C S1C IPC A1C STC ITC V1C HIP AMY STR MDT CBC
M
Corr. = - 0.018, n = 244
P-value = 0.782
NHE9 expression (Log2 RPKM)
CREB1 expression (Log2 RPKM)

cerebellar and cortical mass, prominent glial pathology, and hyperphosphorylated Tau deposition (3, 51–53). Recent revelations on the shared pathology of defective Aβ clearance and altered processing of amyloid precursor protein between autism and Alzheimer's disease suggest that endosomal pH regulation may be one critical mechanistic link between neurodevelopmental and neurodegenerative disorders (54). NHE6 gene expression is depressed in both AD and autism (55, 56). CRE-mediated transcriptional regulation of NHE6 expression offers opportunities to expand the repertoire of drugs that could potentially correct human pathologies resulting from NHE6 down-regulation and aberrant endosomal hyperacidification (Fig. 8*A*). For example, rolipram, a PDE4 inhibitor that elevates cAMP levels, resulting in CREB activation, has shown efficacy as memory enhancer and for amelioration of Aβ-related neuropathology in mouse models (57).

We used mouse astrocytes with knock-in of human ApoE alleles that alter genetic risk for Alzheimer's disease (58). Recently, we showed that NHE6 expression is severely reduced in astrocytes carrying the pathological apoE4 variant, relative to the isogenic nonrisk ApoE3 allele (8). Consistent with this observation, CREB is down-regulated in apoE4 brains (59). First, we confirmed CREB-mediated NHE6 regulation in apoE3 astrocytes using the CREB inhibitor (KG501); we observed dose-dependent down-regulation of NHE6 transcript levels with KG501 treatment (Fig. 8*B*). Rolipram was effective in dose-dependent activation of CREB targets in apoE4 astrocytes, including the prototypic CREB target BDNF (Fig. S7*A*), and astrocyte-specific CREB targets, ALDH1A1 and FBXO2 (60) (Fig. S7, *B* and *C*). We observed significant induction of CREB mRNA by rolipram as well (Fig. 8*C*), consistent with similar observations in rat hippocampus (61). Here, we demonstrate a dose-dependent increase in NHE6 transcript levels with rolipram treatment (1.25–10 μM) in apoE4 astrocytes (Fig. 8*D*). To evaluate the efficacy of rolipram treatment on NHE6-mediated function, we monitored Aβ clearance by endocytosis in cultured apoE4 astrocytes. Cell-associated Aβ was monitored using flow cytometry and confocal microscopy following a short (1-h) incubation with fluorescently tagged peptide (58, 62) (Fig. 8*E*). We show that rolipram elicits a significant increase in Aβ clearance, evidenced by an increase in cell-associated fluorescence by flow cytometry of apoE4 astrocytes (Fig. 8*F*). Similarly, endocytosed Aβ, monitored by confocal microscopy, exhibited an average of 2.66-fold increase following treatment with rolipram (Fig. 8, *G* and *H*). Although the increase in cell-associated Aβ could be, in part, due to a reduction in Aβ degradation, especially at longer time points, our experimental conditions are consistent with increased Aβ uptake. Taken together, our findings suggest that CREB activation of NHE6 expression is translatable into correction of Aβ clearance deficits in apoE4 astrocytes.

Discussion

Nutrient control of endolysosomal pH

The discovery of eNHE in the mid-1990s and subsequent work in a range of model organisms and mammalian systems have established the fundamental importance of these ion transporters in human health and disease (3, 63). Although the contribution of the V-ATPase in nutrient control of endolysosomal pH is well established in yeast (20, 21), the role of eNHE in this mechanism was previously unknown. Here, we leveraged public data from yeast, fly, and mammalian studies to make an unbiased *in silico* prediction leading to the discovery of an evolutionarily conserved mechanism for regulation of eNHE expression by nutrients and HDACs. Previous studies have established that glucose triggers rapid, post-translational regulation of disassembly and reassembly of V-ATPase to regulate the pH gradient across yeast vacuoles (20, 21). In this study, we show that glucose also elicits reciprocal transcriptional changes in Nhx1 and V-ATPase subunits to control vacuolar pH. This finding is in agreement with previous work showing severely reduced survival of Nhx1 mutants during nutrient-depleted stationary phase (19).

The regulation of endolysosomal pH by Nhx1 and V-ATPase (or their orthologs in higher eukaryotes) might promote cell survival during nutrient depletion or starvation by at least three potential mechanisms, as follows. (i) Vacuole acidity facilitates proton-dependent import of amino acids into the lumen through Avt1, a neutral amino acid transporter important for starvation resistance (18, 64). In nutrient-depleted cells, a decrease in vacuolar acidification would reduce vacuolar import of amino acids and help maintain cytoplasmic amino acid homeostasis (Fig. S8, *A* and *B*). (ii) Transcriptional control of V-ATPase subunits could supplement post-translational mechanisms of V-ATPase disassembly as an energy-saving mechanism to conserve ATP under nutrient-limiting conditions. (iii) We have previously shown that Nhx1 regulates vesi-

Figure 7. CREB-mediated transcriptional regulation of NHE6 expression. *A*, experimental framework to directly test whether NHE6 is a CREB target. FLAG-tagged CREB1 plasmid was expressed in HEK293 cells and (i) NHE6 expression and its functional outcome (elevation of endosomal pH) and (ii) binding of CREB to NHE6 promoter by ChIP-qPCR were assessed. *B* and *C*, expression of CREB1 in HEK293 cells significantly elevated NHE6 transcript (****, $p < 0.0001$; $n = 3$; Student's *t* test; *B*), resulting in alkalization of endosomal pH from 5.9 $\pm$ 0.03 to 6.12 $\pm$ 0.05 (**, $p = 0.0075$; $n = 3$; Student's *t* test; *C*). No changes in NHE6 transcript ($p = 0.636$; $n = 3$; Student's *t* test; *B*) or endosomal pH ($p = 0.916$; $n = 3$; Student's *t* test; *C*) were observed with the nonphosphorylatable mutant of CREB1 (S133A). *D* and *E*, schematic of NHE6 (*top*; *D*) and NHE9 (*bottom*; *E*) promoter element showing transcription start site, CREB-binding sites, and locations of ChIP-qPCR assays. *F–H*, ChIP-qPCR amplification of three predicted CREB-binding sites in the promoter of NHE6 at positions -12, $+1$, and $+2$ kb relative to the TSS in HEK293 cells. Note significant CREB binding to the NHE6 promoter at all three predicted sites. *I*, no significant binding of CREB to NHE9 promoter was identified using a primer targeting position -1 kb relative to the TSS. *J*, Western blotting to confirm specific pulldown of CREB1 by probing the ChIP samples from HEK293 cells with an antibody against CREB raised in rabbits. ChIP was performed using an antibody raised in mice. Note the high-molecular weight smear due to formaldehyde cross-linking. *K* and *L*, the pattern of NHE6 expression closely parallels that of CREB1 through normal human brain development (*K*) (Pearson correlation, 0.62; $n = 244$; ****, $p < 0.0001$) and in all areas of the brain (*L*). *DFC*, dorsolateral prefrontal cortex (CTX) (Brodmann area 9 (BA9), BA46); *VFC*, ventrolateral prefrontal CTX (BA44, BA45); *MFC*, medial prefrontal CTX (BA32, BA33, BA34); *OFC*, orbital frontal CTX (BA11); *M1C*, primary motor CTX (BA4); *S1C*, primary somatosensory CTX (BA1-BA3); *IPC*, posterior inferior parietal CTX (BA40); *A1C*, primary auditory CTX (BA41); *STC*, posterior superior temporal CTX (BA22); *ITC*, inferior temporal CTX (BA20); *V1C*, primary visual CTX (BA17); *HIP*, hippocampal formation; *AMY*, amygdaloid complex; *STR*, striatum; *MDT*, mediodorsal nucleus of thalamus; *CBC*, cerebellar CTX. *M*, NHE9 expression showed no correlation with CREB1 (Pearson correlation, -0.018; $n = 244$; $p = 0.782$). Data were obtained from the Allen Brain atlas. *NS*, not significant. *Error bars*, S.D. See related Fig. S6.

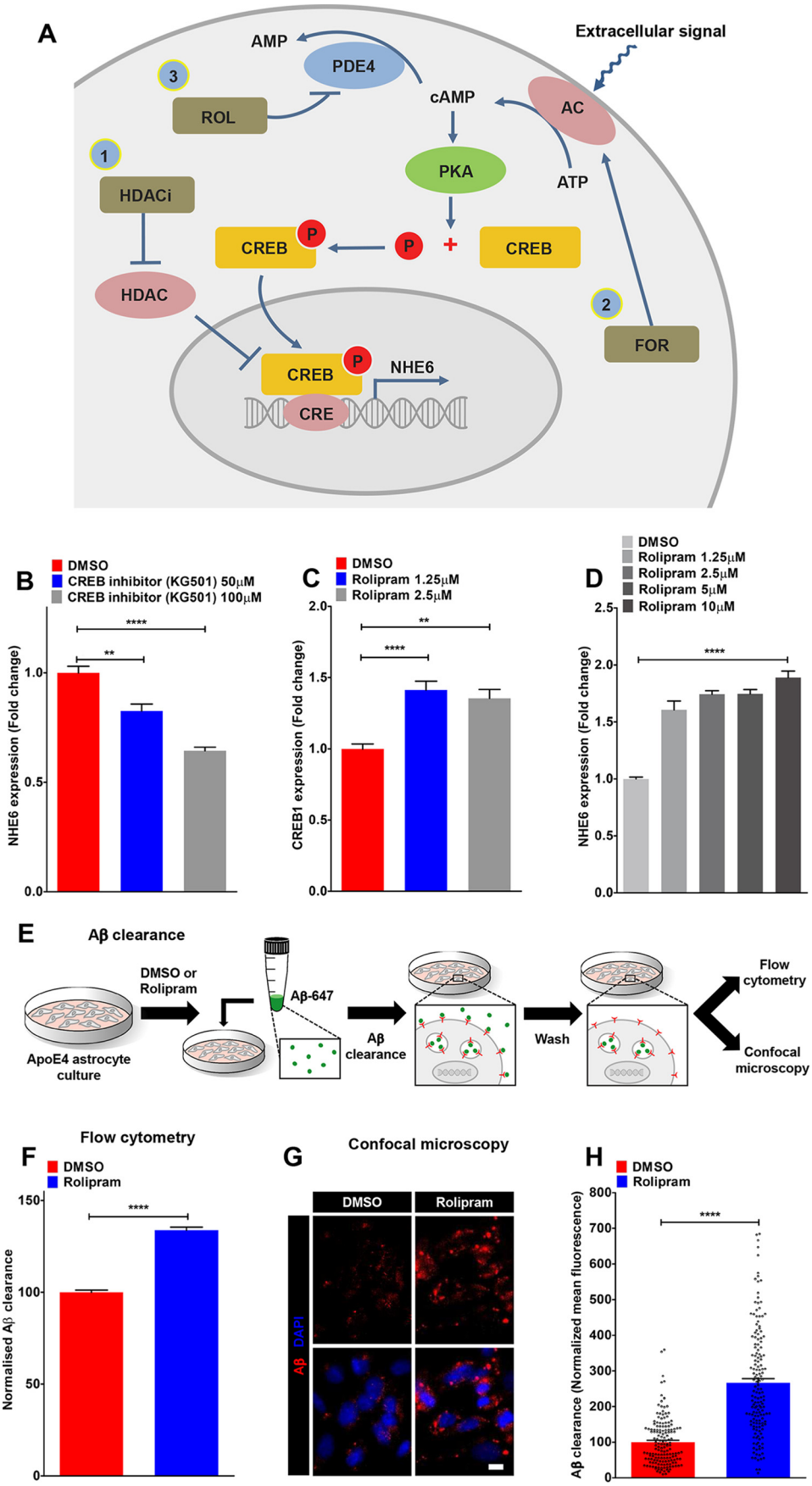
A
AMP
PDE4
3
ROL
cAMP
Extracellular signal
AC
1
HDACi
PKA
ATP
CREB
P
P
+
CREB
HDAC
2
FOR
CREB
P
NHE6
CRE
B
DMSO
CREB inhibitor (KG501) 50μM
CREB inhibitor (KG501) 100μM
NHE6 expression (Fold change)
C
DMSO
Rolipram 1.25μM
Rolipram 2.5μM
CREB1 expression (Fold change)
D
DMSO
Rolipram 1.25μM
Rolipram 2.5μM
Rolipram 5μM
Rolipram 10μM
NHE6 expression (Fold change)
E
Aβ clearance
DMSO or Rolipram
Aβ-647
ApoE4 astrocyte culture
Aβ clearance
Wash
Flow cytometry
Confocal microscopy
F
Flow cytometry
DMSO
Rolipram
Normalised Aβ clearance
G
Confocal microscopy
DMSO
Rolipram
Aβ DAPI
H
DMSO
Rolipram
Aβ clearance (Normalized mean fluorescence)

cle trafficking and lysosomal biogenesis to control internalization of plasma membrane proteins and degradation in vacuoles (15, 63). Increased Nhx1 expression in glucose-depleted cells might therefore help promote endocytosis and provide resources for survival during glucose starvation (65). Intriguingly, eNHE mutants in *Caenorhabditis elegans* (Nhx5) and fly (DmNHE3) were found to be resistant to metformin, a biguanide drug commonly used to treat type-2 diabetes, potentially through dysregulation of autophagy (66). Given that metformin is known to induce a caloric restriction-like state (67), our findings suggest that up-regulation of eNHE and alkalinization of endosomal pH may underlie response to metformin therapy.

Antifungal drugs target endolysosomal pH

Pathogenic fungi have become a leading cause of morbidity and mortality in the world (68). Fungi need V-ATPase function to infect their hosts, and genetic inactivation of vacuole-specific V_o subunit Vph1, but not secretory pathway-specific subunit Stv1, abolished virulence and invasive growth of *C. albicans*, underscoring the importance of endolysosomal pH as a drug target (16, 17). Consistent with this finding, the antifungal activity of azoles, which inhibit biosynthesis of fungus-specific sterol, ergosterol, is mediated by reduced V-ATPase activity in ergosterol-deficient vacuoles (31). Similarly, decreased V-ATPase activity may underlie the antifungal activity of amphotericin B, which is known to directly bind and sequester ergosterol in yeast cells (69). Furthermore, many naturally occurring antifungal compounds, such as terpenoid phenols, function at least in part by disrupting V-ATPase function (70). Recent studies have documented the potential benefits of repurposing FDA-approved amphipathic drugs, such as amiodarone, already in clinical use as calcium antagonists, that partition into acidic compartments, alkalinize endolysosomes, and potentiate antifungal effects and reverse resistance to azole drugs (71). Here we show that an antifungal HDAC inhibitor, TSA, increases vacuole pH and enhances the antifungal effects of fluconazole. Intriguingly, both amiodarone and HDAC inhibitors confer significant neuroprotection in cell culture and animal models (11, 12, 72). Together, these studies and our current findings makes a strong case for (i) repurposing antifungal drugs as potential drugs to correct human pathologies arising from dysregulation of endolysosomal pH and (ii) repurposing FDA-approved drugs having off-target effects on pH homeostasis as candidates for the development of new therapeutic strategies for fungal disease.

Targeting endolysosomal pH in human diseases

Dysregulation of endolysosomal pH is an emerging theme in pathogenesis of a wide range of human diseases, ranging from neurodegeneration to cancer (7, 73). There is clearly potential for intervention to exploit the disease-modifying effects of endosomal pH, and this should be investigated further. From lessons learned with bakers' yeast, we know that gene disruption of *NHX1* leads to cellular phenotypes reminiscent of Alzheimer's disease (AD) that include an enlarged endosome/prevacuolar compartment, hyperacidic luminal pH, enhanced proteolysis of the chaperone protein Vps10 (a homolog of the AD susceptibility factor SORL1), mistrafficking of vacuolar hydrolases, and profound deficiencies in lysosomal cargo delivery (15, 74). Several studies have identified links between eNHE and a host of neurological disorders, including autism, intellectual disability, epilepsy, Parkinson's disease, multiple sclerosis, and more recently late-onset AD (3, 8, 55, 75), although mechanisms underlying eNHE regulation have remained obscure. Here we show that expression of the Christianson syndrome protein NHE6 is under the control of CREB transcription factor. A translatable finding from our studies is that pharmacological HDAC inhibition (by TSA) or CREB activation (by forskolin or rolipram) elevates endosomal pH and has the potential to mitigate human pathologies, such as AD and autism, associated with aberrant endosomal hyperacidification. Furthermore, regulation of endolysosomal pH may at least partially explain the working mechanism of HDAC inhibitors in cancer therapy. Tumor cells in the periphery have better blood supply, whereas cells inside tumor masses are under starved conditions, because nutrients are not fully supplied to these cells. As we have shown earlier, a subset of brain cancer glioblastoma multiforme show significant up-regulation of eNHE isoform NHE9 that might help in the survival of tumor cells in nutrient-limited conditions (76). Together, these data suggest that, by governing fundamentally critical endosomal pH homeostasis, eNHE plays an important role in mediating nutrient control of endolysosomal pH. This importance makes them an attractive target as antifungal drugs and in several human diseases. Exploration of the conserved mechanism for regulation of endolysosomal pH by histone deacetylases provides a foundation for understanding the pathways regulating pH homeostasis and a platform for the development of drugs that could potentially correct human pathologies resulting from dysregulated endolysosomal acidification.

Figure 8. Control of NHE6 expression by pharmacological targeting of CREB pathway. *A*, extracellular signals induce adenylyl cyclase, which elevates cAMP levels and activates the cAMP-dependent protein kinase A (*PKA*), which in turn induces CREB phosphorylation at serine 133. Active phospho-CREB translocates to the nucleus and activates transcription of NHE6, which contains CRE in its promoter. At least three different pharmacological approaches could be used to activate CREB and enhance NHE6 transcription. First, HDAC inhibitors (*HDACi*) activate CREB by attenuating HDAC-mediated repression. Second, forskolin (*FOR*), an agonist of adenylyl cyclase, stimulates production of cAMP and activates CREB. Third, rolipram (*ROL*), a PDE4 inhibitor, inhibits hydrolysis of cAMP and activates CREB. *B*, qPCR analysis to confirm CREB-mediated NHE6 regulation in apoE3 astrocytes using the CREB inhibitor (KG501). Note the dose-dependent down-regulation of NHE6 transcript levels with KG501 treatment (****, $p < 0.0001$; $n = 3$; Student's *t* test). *C*, qPCR analysis demonstrating dose-dependent increase in CREB1 transcript levels with rolipram treatment in apoE4 astrocytes. *D*, qPCR analysis to demonstrate dose-dependent increase in NHE6 transcript levels with rolipram treatment (1.25–10 μM) in apoE4 astrocytes (****, $p < 0.0001$; $n = 3$; Student's *t* test). *E*, fluorescence-based assay to monitor clearance of Aβ peptides by apoE4 astrocytes. *F*, quantitation of Aβ clearance from FACS analysis of 10,000 cells in biological triplicates confirmed restoration of Aβ clearance in apoE4 astrocytes with rolipram treatment (****, $p < 0.0001$; $n = 3$; Student's *t* test). *G* and *H*, representative micrographs (*G*) and quantification (*H*) showing a ~2.66-fold increase in cell-associated Aβ in apoE4 astrocytes with rolipram treatment (****, $p < 0.0001$; $n = 160$/condition; Student's *t* test). *Error bars*, S.D. See related Fig. S7.

Experimental procedures

Yeast strains and growth

All *S. cerevisiae* strains used were derivatives of BY4741 (a gift from Dr. Susan Michaelis (The Johns Hopkins University) or purchased from transOMIC Technologies). Yeast cells were grown in YPD (yeast extract, peptone, and dextrose) medium at 30 °C with shaking at 250 rpm. Acute glucose depletion was performed by growing yeast in in YP (yeast extract and peptone) medium. Yeast growth was determined by A_{600}. A spotting assay on YPD agar plates was performed to detect drug-induced growth inhibition phenotypes.

Alkaline pH sensitivity and quinacrine staining

Increased luminal pH in the yeast vacuole was detected using two defining phenotypes: alkaline pH sensitivity and loss of quinacrine fluorescence. Sensitivity to alkaline medium pH was assayed in YPD medium, which was adjusted to pH 7 or pH 4.3. For quinacrine staining, cells were suspended in YPD medium containing 100 mM HEPES, pH 7.6, 200 μM quinacrine and stained for 10 min at 30 °C. Stained cells were washed three times with 100 mM HEPES, pH 7.6, 0.2% glucose and examined by fluorescence microscopy immediately. Quantification of images was done using ImageJ software.

Cell culture

Human ApoE isoform-expressing (apoE3 and apoE4) immortalized astrocytes (gift from Dr. David M Holtzman, Washington University, St. Louis) were maintained in DMEM/F-12 (Invitrogen) supplemented with 10% fetal bovine serum (Invitrogen) and 200 μg/ml Geneticin/G418 (Corning Cellgro). HEK293T cells were obtained from ATCC and grown in DMEM/high glucose/sodium pyruvate (Invitrogen) containing 10% fetal bovine serum. Culture conditions were in a 5% CO_2 incubator at 37 °C. Cell viability was measured using the trypan blue exclusion method.

Aβ clearance assays

To quantify Aβ clearance, apoE4 astrocytes were washed with serum-free medium followed by incubation with 100 nM fluorescently labeled HiLyte Fluor 647-Aβ40 (AS-64161, AnaSpec). Following several washes with PBS, cells were fixed for confocal imaging using the LSM 700 confocal microscope (Zeiss) or trypsinized for flow cytometry analysis of ~10,000 cells in biological triplicates using the FACSCalibur instrument (BD Biosciences). Unstained cells without any exposure to fluorescently labeled Aβ were used as a control for background fluorescence. Quantification of confocal images was done using ImageJ software.

Antibodies and reagents

ChIP grade mouse monoclonal anti-FLAG (M2) (F3165) and rabbit monoclonal anti-CREB (48H2) (9197) were obtained from Sigma and Cell Signaling Technology, respectively. TSA (A8183) was from ApexBio Technology. Concanamycin A (C9705), fluconazole (F8929), KG501 (70485), and rolipram (R6520) were obtained from Sigma. Forskolin (3828) was purchased from Cell Signaling Technology.

Plasmids and transfection

pBY011 Rpd3 plasmid under galactose inducible promoter was obtained from Harvard PlasmID Repository (ScCD00010538). Empty vector with uracil resistance was a gift of Dr. Steven Claypool (The Johns Hopkins University). Yeast transformation was performed using the lithium acetate method. pCF CREB1 (Addgene plasmid 22968) and pCF CREB1 S133A (Addgene plasmid 22969) were a gift from Dr. Marc Montminy. pcDNA-HDAC4 (S246A/S467A/S632A) (Addgene plasmid 30486) was a gift from Dr. Tso-Pang Yao. HEK293T cells were transfected using Lipofectamine 2000 reagent as per the manufacturer's instructions.

Quantitative real-time PCR

mRNA was extracted from yeast and cell cultures using the RNeasy minikit (74104, Qiagen) with DNase I (10104159001, Roche Applied Science) treatment, following the manufacturer's instructions. Yeast lysis buffer contained 1 M sorbitol, 0.1 M EDTA, 0.1% β-mercaptoethanol, and zymolase (E1004, Zymo Research). Complementary DNA was synthesized using the high-capacity RNA-to-cDNA kit (4387406, Applied Biosystems). Quantitative real-time PCR analysis was performed using the 7500 real-time PCR system (Applied Biosystems) using Taqman Fast universal PCR Master Mix (4352042, Applied Biosystems). Taqman gene expression assay probes used in this study are as follows: yeast: ACT1, Sc04120488_s1; NHX1, Sc04115315_s1; RPD3, Sc04161394_s1; STV1, Sc04153492_s1; VMA1, Sc04108170_s1; VMA7, Sc04124849_s1; human: ATP6V0A1, Hs00989334_m1; ATP6V0A2, Hs00429389_m1; GAPDH, Hs02786624_g1; NHE6, Hs00234723_m1; NHE7, Hs01078624_m1; NHE9, Hs00543518_m1; mouse: ALDH1A1, Mm00657317_m1; BDNF, Mm04230607_s1; CREB1, Mm00501607_m1; FBXO2, Mm00805188_g1; GAPDH, Mm99999915_g1; NHE6, Mm00555445_m1. The *Ct* (cycle threshold) values were first normalized to endogenous control levels by calculating the ΔCt for each sample. These values were then analyzed relative to control, to generate a $\Delta\Delta Ct$ value. -Fold change was obtained using the equation, expression -fold change $= 2^{-\Delta\Delta Ct}$. Each experiment was repeated three times independently.

Endosomal pH measurement

Endosomal pH was measured using flow cytometry, as we described previously (55, 75). Briefly, cells were rinsed and incubated in serum-free medium for 30 min to remove residual transferrin and then incubated with pH-sensitive FITC-transferrin (T2871, Thermo Fisher Scientific) (75 μg/ml) together with pH-nonsensitive Alexa Fluor 633–transferrin (T23362, Thermo Fisher Scientific) (25 μg/ml) at 37 °C for 1 h. Cells were placed on ice to stop transferrin uptake, and excess transferrin was removed by washing twice with ice-cold serum-free DMEM and PBS. Bound transferrin was removed by washing with ice-cold PBS, pH 5.0, and PBS, pH 7.0. Cells were trypsinized, and pH was determined by flow cytometry analysis of ~10,000 cells in biological triplicates using the FACSCalibur instrument (BD Biosciences). A four-point calibration curve with different pH values (4.5, 5.5, 6.5, and 7.5) was generated using the Intracellular pH Calibration Buffer Kit (P35379,

Thermo Fisher Scientific) in the presence of 10 μM K^+/H^+ ionophore nigericin and 10 μM K^+ ionophore valinomycin.

Bioinformatics

An unbiased *in silico* approach was used to identify experimental conditions that significantly altered Nhx1 expression, by analyzing data from 284 *Saccharomyces cerevisiae* microarray studies, which comprised a wide range of studies, including gene deletion, overexpression and mutations, drug/toxin treatment, nutrient limitation or excess, metabolic/environmental stress, and many others. Experimental conditions with a minimum gene expression -fold change of ±2 were selected for further thorough pathway analysis. A predictive model for regulation of Nhx1 expression was created based on the overlap of pathways from experimental conditions that resulted in the highest degree of changes in gene expression (both up- and down-regulation) and selected for *in vitro* validation. Meta-analysis of 45 microarray experiments, including 937 samples, determined the effect of growth phase on Nhx1 expression. Normalized yeast expression data were obtained from Genevestigator (Nebion AG). *Drosophila* microarray experiment GSE14531 was analyzed to study the starvation effect on fly larvae. Mammalian gene expression data sets included in the study were GSE11291, GSE8488, and GSE9247. Human brain and *Drosophila* gene expression data were obtained from the Allen Brain and FlyBase atlas, respectively.

ChIP-qPCR

To assess physical binding of the FLAG-tagged CREB to the NHE6 gene promoter, ChIP-qPCR was carried out. ChIP was performed using the EpiQuik ChIP kit (P-2002, Epigentek), according to the manufacturer's instructions. In brief, cells were treated with 1% formaldehyde for 10 min to cross-link proteins to DNA. To generate DNA fragments ~200–1,000 base pairs long, the cross-linked chromatin was sonicated on ice. ChIP assays were performed using a ChIP grade anti-FLAG antibody. Specific pulldown of CREB1 was confirmed by probing the ChIP samples with an antibody against CREB raised in rabbits using Western blotting. After reversal of the cross-links, qPCR was performed using the EpiTect ChIP-qPCR primer assay for NHE6/*SLC9A6* (GPH1013950(−)12A, −12 kb from the transcription start site; GPH1013950(+)01A, +1 kb from the transcription start site; and GPH1013950(+)02A, +2 kb from the transcription start site). The ChIP-qPCR primer assay for the NHE9/*SLC9A9* promoter (GPH1023313(−)01A, −1 kb from the transcription start site) was used as a control (all Qiagen). The resulting amplification and melt curves were analyzed to ensure specific PCR product. *Ct* values were used to calculate the -fold enhancement.

Luciferase assay

pCRE-Luc (encoding for CRE and firefly luciferase) and pSV40-RL (encoding for an SV40 promoter and *Renilla* luciferase) plasmids (gift of Dr. Jennifer L. Pluznick, The Johns Hopkins University) were transiently transfected into HEK293T cells using Lipofectamine 2000 reagent, as per the manufacturer's instructions. The ratio of firefly luciferase and *Renilla* luciferase was measured using the Dual-Luciferase assay system (E1910, Promega) with data collected using a FLUOstar Omega automated plate reader (BMG LabTech) to evaluate the CREB activation following treatment with an HDAC inhibitor.

Author contributions—H. P. designed, conducted, and analyzed experiments and wrote the paper. R. R. designed and interpreted experiments and wrote the paper.

Acknowledgments—We thank Dr. David M. Holtzman (Washington University, St. Louis, MO) for the gift of apoE immortalized astrocytes. We thank Dr. Susan Michaelis, Dr. Steven Claypool, and Dr. Jennifer L. Pluznick (The Johns Hopkins University) for yeast strains and plasmids.

References

1. Maxfield, F. R. (2014) Role of endosomes and lysosomes in human disease. *Cold Spring Harb. Perspect. Biol.* **6,** a016931 CrossRef Medline
2. Casey, J. R., Grinstein, S., and Orlowski, J. (2010) Sensors and regulators of intracellular pH. *Nat. Rev. Mol. Cell Biol.* **11,** 50–61 CrossRef Medline
3. Kondapalli, K. C., Prasad, H., and Rao, R. (2014) An inside job: how endosomal Na^+/H^+ exchangers link to autism and neurological disease. *Front. Cell. Neurosci.* **8,** 172 Medline
4. Picollo, A., and Pusch, M. (2005) Chloride/proton antiporter activity of mammalian CLC proteins ClC-4 and ClC-5. *Nature* **436,** 420–423 CrossRef Medline
5. Lee, C., Kang, H. J., von Ballmoos, C., Newstead, S., Uzdavinys, P., Dotson, D. L., Iwata, S., Beckstein, O., Cameron, A. D., and Drew, D. (2013) A two-domain elevator mechanism for sodium/proton antiport. *Nature* **501,** 573–577 CrossRef Medline
6. Esmail, S., Kartner, N., Yao, Y., Kim, J. W., Reithmeier, R. A. F., and Manolson, M. F. (2018) Molecular mechanisms of cutis laxa and distal renal tubular acidosis-causing mutations in V-ATPase a subunits, ATP6V0A2 and ATP6V0A4. *J. Biol. Chem.* **293,** 2787–2800 CrossRef Medline
7. Colacurcio, D. J., and Nixon, R. A. (2016) Disorders of lysosomal acidification: the emerging role of v-ATPase in aging and neurodegenerative disease. *Ageing Res. Rev.* **32,** 75–88 CrossRef Medline
8. Prasad, H., and Rao, R. (2018) The amyloid clearance defect in apoE4 astrocytes is corrected by epigenetic restoration of NHE6. *bioRxiv* 243097 CrossRef
9. Treusch, S., Hamamichi, S., Goodman, J. L., Matlack, K. E., Chung, C. Y., Baru, V., Shulman, J. M., Parrado, A., Bevis, B. J., Valastyan, J. S., Han, H., Lindhagen-Persson, M., Reiman, E. M., Evans, D. A., Bennett, D. A., *et al.* (2011) Functional links between Abeta toxicity, endocytic trafficking, and Alzheimer's disease risk factors in yeast. *Science* **334,** 1241–1245 CrossRef Medline
10. Seto, E., and Yoshida, M. (2014) Erasers of histone acetylation: the histone deacetylase enzymes. *Cold Spring Harb. Perspect. Biol.* **6,** a018713 CrossRef Medline
11. Gräff, J., Rei, D., Guan, J. S., Wang, W. Y., Seo, J., Hennig, K. M., Nieland, T. J., Fass, D. M., Kao, P. F., Kahn, M., Su, S. C., Samiei, A., Joseph, N., Haggarty, S. J., Delalle, I., and Tsai, L. H. (2012) An epigenetic blockade of cognitive functions in the neurodegenerating brain. *Nature* **483,** 222–226 CrossRef Medline
12. Vecsey, C. G., Hawk, J. D., Lattal, K. M., Stein, J. M., Fabian, S. A., Attner, M. A., Cabrera, S. M., McDonough, C. B., Brindle, P. K., Abel, T., and Wood, M. A. (2007) Histone deacetylase inhibitors enhance memory and synaptic plasticity via CREB:CBP-dependent transcriptional activation. *J. Neurosci.* **27,** 6128–6140 CrossRef Medline
13. Makena, M. R., Koneru, B., Nguyen, T. H., Kang, M. H., and Reynolds, C. P. (2017) Reactive oxygen species-mediated synergism of fenretinide and romidepsin in preclinical models of T-cell lymphoid malignancies. *Mol. Cancer Ther.* **16,** 649–661 CrossRef Medline
14. Dinarello, C. A., Fossati, G., and Mascagni, P. (2011) Histone deacetylase inhibitors for treating a spectrum of diseases not related to cancer. *Mol. Med.* **17,** 333–352 CrossRef Medline

15. Brett, C. L., Tukaye, D. N., Mukherjee, S., and Rao, R. (2005) The yeast endosomal Na^+K^+/H^+ exchanger Nhx1 regulates cellular pH to control vesicle trafficking. *Mol. Biol. Cell* **16,** 1396–1405 CrossRef Medline
16. Patenaude, C., Zhang, Y., Cormack, B., Köhler, J., and Rao, R. (2013) Essential role for vacuolar acidification in *Candida albicans* virulence. *J. Biol. Chem.* **288,** 26256–26264 CrossRef Medline
17. Tarsio, M., Zheng, H., Smardon, A. M., Martínez-Muñoz, G. A., and Kane, P. M. (2011) Consequences of loss of Vph1 protein-containing vacuolar ATPases (V-ATPases) for overall cellular pH homeostasis. *J. Biol. Chem.* **286,** 28089–28096 CrossRef Medline
18. Hughes, A. L., and Gottschling, D. E. (2012) An early age increase in vacuolar pH limits mitochondrial function and lifespan in yeast. *Nature* **492,** 261–265 CrossRef Medline
19. Numata, M., Petrecca, K., Lake, N., and Orlowski, J. (1998) Identification of a mitochondrial Na^+/H^+ exchanger. *J. Biol. Chem.* **273,** 6951–6959 CrossRef Medline
20. Kane, P. M. (1995) Disassembly and reassembly of the yeast vacuolar H^+-ATPase *in vivo*. *J. Biol. Chem.* **270,** 17025–17032 Medline
21. Kane, P. M., and Parra, K. J. (2000) Assembly and regulation of the yeast vacuolar H^+-ATPase. *J. Exp. Biol.* **203,** 81–87 Medline
22. Pnueli, L., Edry, I., Cohen, M., and Kassir, Y. (2004) Glucose and nitrogen regulate the switch from histone deacetylation to acetylation for expression of early meiosis-specific genes in budding yeast. *Mol. Cell. Biol.* **24,** 5197–5208 CrossRef Medline
23. Bernstein, B. E., Tong, J. K., and Schreiber, S. L. (2000) Genomewide studies of histone deacetylase function in yeast. *Proc. Natl. Acad. Sci. U.S.A.* **97,** 13708–13713 CrossRef Medline
24. Kim, S., Benguria, A., Lai, C. Y., and Jazwinski, S. M. (1999) Modulation of life-span by histone deacetylase genes in *Saccharomyces cerevisiae*. *Mol. Biol. Cell* **10,** 3125–3136 CrossRef Medline
25. Leonov, A., Feldman, R., Piano, A., Arlia-Ciommo, A., Lutchman, V., Ahmadi, M., Elsaser, S., Fakim, H., Heshmati-Moghaddam, M., Hussain, A., Orfali, S., Rajen, H., Roofigari-Esfahani, N., Rosanelli, L., and Titorenko, V. I. (2017) Caloric restriction extends yeast chronological lifespan via a mechanism linking cellular aging to cell cycle regulation, maintenance of a quiescent state, entry into a non-quiescent state and survival in the non-quiescent state. *Oncotarget* **8,** 69328–69350 Medline
26. Deckert, J., and Struhl, K. (2002) Targeted recruitment of Rpd3 histone deacetylase represses transcription by inhibiting recruitment of Swi/Snf, SAGA, and TATA binding protein. *Mol. Cell. Biol.* **22,** 6458–6470 CrossRef Medline
27. Yarragudi, A., Parfrey, L. W., and Morse, R. H. (2007) Genome-wide analysis of transcriptional dependence and probable target sites for Abf1 and Rap1 in *Saccharomyces cerevisiae*. *Nucleic Acids Res.* **35,** 193–202 CrossRef Medline
28. Bosio, M. C., Fermi, B., Spagnoli, G., Levati, E., Rubbi, L., Ferrari, R., Pellegrini, M., and Dieci, G. (2017) Abf1 and other general regulatory factors control ribosome biogenesis gene expression in budding yeast. *Nucleic Acids Res.* **45,** 4493–4506 CrossRef Medline
29. Fermi, B., Bosio, M. C., and Dieci, G. (2016) Promoter architecture and transcriptional regulation of Abf1-dependent ribosomal protein genes in *Saccharomyces cerevisiae*. *Nucleic Acids Res.* **44,** 6113–6126 CrossRef Medline
30. MacIsaac, K. D., Wang, T., Gordon, D. B., Gifford, D. K., Stormo, G. D., and Fraenkel, E. (2006) An improved map of conserved regulatory sites for *Saccharomyces cerevisiae*. *BMC Bioinformatics* **7,** 113 CrossRef Medline
31. Zhang, Y. Q., Gamarra, S., Garcia-Effron, G., Park, S., Perlin, D. S., and Rao, R. (2010) Requirement for ergosterol in V-ATPase function underlies antifungal activity of azole drugs. *PLoS Pathogens* **6,** e1000939 CrossRef Medline
32. Sambade, M., Alba, M., Smardon, A. M., West, R. W., and Kane, P. M. (2005) A genomic screen for yeast vacuolar membrane ATPase mutants. *Genetics* **170,** 1539–1551 CrossRef Medline
33. Brett, C. L., Donowitz, M., and Rao, R. (2005) Evolutionary origins of eukaryotic sodium/proton exchangers. *Am. J. Physiol. Cell Physiol.* **288,** C223–C239 CrossRef Medline
34. Palanker, L., Tennessen, J. M., Lam, G., and Thummel, C. S. (2009) *Drosophila* HNF4 regulates lipid mobilization and β-oxidation. *Cell Metab.* **9,** 228–239 CrossRef Medline
35. Mihaylova, M. M., Vasquez, D. S., Ravnskjaer, K., Denechaud, P. D., Yu, R. T., Alvarez, J. G., Downes, M., Evans, R. M., Montminy, M., and Shaw, R. J. (2011) Class IIa histone deacetylases are hormone-activated regulators of FOXO and mammalian glucose homeostasis. *Cell* **145,** 607–621 CrossRef Medline
36. Johnson, M. L., Distelmaier, K., Lanza, I. R., Irving, B. A., Robinson, M. M., Konopka, A. R., Shulman, G. I., and Nair, K. S. (2016) Mechanism by which caloric restriction improves insulin sensitivity in sedentary obese adults. *Diabetes* **65,** 74–84 Medline
37. Li, Y., Daniel, M., and Tollefsbol, T. O. (2011) Epigenetic regulation of caloric restriction in aging. *BMC Med.* **9,** 98 CrossRef Medline
38. Wheatley, K. E., Nogueira, L. M., Perkins, S. N., and Hursting, S. D. (2011) Differential effects of calorie restriction and exercise on the adipose transcriptome in diet-induced obese mice. *J. Obes.* **2011,** 265417 CrossRef Medline
39. Fusco, S., Ripoli, C., Podda, M. V., Ranieri, S. C., Leone, L., Toietta, G., McBurney, M. W., Schütz, G., Riccio, A., Grassi, C., Galeotti, T., and Pani, G. (2012) A role for neuronal cAMP responsive-element binding (CREB)-1 in brain responses to calorie restriction. *Proc. Natl. Acad. Sci. U.S.A.* **109,** 621–626 CrossRef Medline
40. Prior, M. J., Larance, M., Lawrence, R. T., Soul, J., Humphrey, S., Burchfield, J., Kistler, C., Davey, J. R., La-Borde, P. J., Buckley, M., Kanazawa, H., Parton, R. G., Guilhaus, M., and James, D. E. (2011) Quantitative proteomic analysis of the adipocyte plasma membrane. *J. Proteome Res.* **10,** 4970–4982 CrossRef Medline
41. Ouyang, Q., Lizarraga, S. B., Schmidt, M., Yang, U., Gong, J., Ellisor, D., Kauer, J. A., and Morrow, E. M. (2013) Christianson syndrome protein NHE6 modulates TrkB endosomal signaling required for neuronal circuit development. *Neuron* **80,** 97–112 CrossRef Medline
42. Walton, M. R., and Dragunow, I. (2000) Is CREB a key to neuronal survival? *Trends Neurosci.* **23,** 48–53 CrossRef Medline
43. Barger, J. L., Kayo, T., Vann, J. M., Arias, E. B., Wang, J., Hacker, T. A., Wang, Y., Raederstorff, D., Morrow, J. D., Leeuwenburgh, C., Allison, D. B., Saupe, K. W., Cartee, G. D., Weindruch, R., and Prolla, T. A. (2008) A low dose of dietary resveratrol partially mimics caloric restriction and retards aging parameters in mice. *PLoS One* **3,** e2264 CrossRef Medline
44. Schroeder, T. M., Nair, A. K., Staggs, R., Lamblin, A. F., and Westendorf, J. J. (2007) Gene profile analysis of osteoblast genes differentially regulated by histone deacetylase inhibitors. *BMC Genomics* **8,** 362 CrossRef Medline
45. Ulici, V., James, C. G., Hoenselaar, K. D., and Beier, F. (2010) Regulation of gene expression by PI3K in mouse growth plate chondrocytes. *PLoS One* **5,** e8866 CrossRef Medline
46. Fusco, S., Leone, L., Barbati, S. A., Samengo, D., Piacentini, R., Maulucci, G., Toietta, G., Spinelli, M., McBurney, M., Pani, G., and Grassi, C. (2016) A CREB-Sirt1-Hes1 circuitry mediates neural stem cell response to glucose availability. *Cell Rep.* **14,** 1195–1205 CrossRef Medline
47. Canettieri, G., Morantte, I., Guzmán, E., Asahara, H., Herzig, S., Anderson, S. D., Yates, J. R., 3rd, Montminy, M. (2003) Attenuation of a phosphorylation-dependent activator by an HDAC-PP1 complex. *Nat. Struct. Biol.* **10,** 175–181 CrossRef Medline
48. Li, J., Chen, J., Ricupero, C. L., Hart, R. P., Schwartz, M. S., Kusnecov, A., and Herrup, K. (2012) Nuclear accumulation of HDAC4 in ATM deficiency promotes neurodegeneration in ataxia telangiectasia. *Nat. Med.* **18,** 783–790 CrossRef Medline
49. Silve, S., Rhode, P. R., Coll, B., Campbell, J., and Poyton, R. O. (1992) ABF1 is a phosphoprotein and plays a role in carbon source control of COX6 transcription in *Saccharomyces cerevisiae*. *Mol. Cell. Biol.* **12,** 4197–4208 CrossRef Medline
50. Zhang, X., Odom, D. T., Koo, S. H., Conkright, M. D., Canettieri, G., Best, J., Chen, H., Jenner, R., Herbolsheimer, E., Jacobsen, E., Kadam, S., Ecker, J. R., Emerson, B., Hogenesch, J. B., Unterman, T., *et al.* (2005) Genome-wide analysis of cAMP-response element binding protein occupancy, phosphorylation, and target gene activation in human tissues. *Proc. Natl. Acad. Sci. U.S.A.* **102,** 4459–4464 CrossRef Medline

51. Garbern, J. Y., Neumann, M., Trojanowski, J. Q., Lee, V. M., Feldman, G., Norris, J. W., Friez, M. J., Schwartz, C. E., Stevenson, R., and Sima, A. A. (2010) A mutation affecting the sodium/proton exchanger, SLC9A6, causes mental retardation with tau deposition. *Brain* **133,** 1391–1402 CrossRef Medline
52. Mignot, C., Héron, D., Bursztyn, J., Momtchilova, M., Mayer, M., Whalen, S., Legall, A., Billette de Villemeur, T., and Burglen, L. (2013) Novel mutation in SLC9A6 gene in a patient with Christianson syndrome and retinitis pigmentosum. *Brain Dev.* **35,** 172–176 CrossRef Medline
53. Strømme, P., Dobrenis, K., Sillitoe, R. V., Gulinello, M., Ali, N. F., Davidson, C., Micsenyi, M. C., Stephney, G., Ellevog, L., Klungland, A., and Walkley, S. U. (2011) X-linked Angelman-like syndrome caused by Slc9a6 knockout in mice exhibits evidence of endosomal-lysosomal dysfunction. *Brain* **134,** 3369–3383 CrossRef Medline
54. Westmark, C. J., Sokol, D. K., Maloney, B., and Lahiri, D. K. (2016) Novel roles of amyloid-β precursor protein metabolites in fragile X syndrome and autism. *Mol. Psychiatry* **21,** 1333–1341 CrossRef Medline
55. Prasad, H., and Rao, R. (2015) The Na^+/H^+ exchanger NHE6 modulates endosomal pH to control processing of amyloid precursor protein in a cell culture model of Alzheimer disease. *J. Biol. Chem.* **290,** 5311–5327 CrossRef Medline
56. Schwede, M., Garbett, K., Mirnics, K., Geschwind, D. H., and Morrow, E. M. (2014) Genes for endosomal NHE6 and NHE9 are misregulated in autism brains. *Mol. Psychiatry* **19,** 277–279 CrossRef Medline
57. Gong, B., Vitolo, O. V., Trinchese, F., Liu, S., Shelanski, M., and Arancio, O. (2004) Persistent improvement in synaptic and cognitive functions in an Alzheimer mouse model after rolipram treatment. *J. Clin. Invest.* **114,** 1624–1634 CrossRef Medline
58. Verghese, P. B., Castellano, J. M., Garai, K., Wang, Y., Jiang, H., Shah, A., Bu, G., Frieden, C., and Holtzman, D. M. (2013) ApoE influences amyloid-β (Aβ) clearance despite minimal apoE/Aβ association in physiological conditions. *Proc. Natl. Acad. Sci. U.S.A.* **110,** E1807–E1816 CrossRef Medline
59. Qiao, F., Gao, X. P., Yuan, L., Cai, H. Y., and Qi, J. S. (2014) Apolipoprotein E4 impairs *in vivo* hippocampal long-term synaptic plasticity by reducing the phosphorylation of CaMKIIα and CREB. *J. Alzheimers Dis.* **41,** 1165–1176 Medline
60. Pardo, L., Schlüter, A., Valor, L. M., Barco, A., Giralt, M., Golbano, A., Hidalgo, J., Jia, P., Zhao, Z., Jové, M., Portero-Otin, M., Ruiz, M., Giménez-Llort, L., Masgrau, R., Pujol, A., and Galea, E. (2016) Targeted activation of CREB in reactive astrocytes is neuroprotective in focal acute cortical injury. *Glia* **64,** 853–874 CrossRef Medline
61. Nibuya, M., Nestler, E. J., and Duman, R. S. (1996) Chronic antidepressant administration increases the expression of cAMP response element binding protein (CREB) in rat hippocampus. *J. Neurosci.* **16,** 2365–2372 Medline
62. Nazer, B., Hong, S., and Selkoe, D. J. (2008) LRP promotes endocytosis and degradation, but not transcytosis, of the amyloid-beta peptide in a blood-brain barrier *in vitro* model. *Neurobiol. Dis.* **30,** 94–102 CrossRef Medline
63. Nass, R., and Rao, R. (1998) Novel localization of a Na^+/H^+ exchanger in a late endosomal compartment of yeast: implications for vacuole biogenesis. *J. Biol. Chem.* **273,** 21054–21060 CrossRef Medline
64. Davey, H. M., Cross, E. J., Davey, C. L., Gkargkas, K., Delneri, D., Hoyle, D. C., Oliver, S. G., Kell, D. B., and Griffith, G. W. (2012) Genome-wide analysis of longevity in nutrient-deprived *Saccharomyces cerevisiae* reveals importance of recycling in maintaining cell viability. *Environ. Microbiol.* **14,** 1249–1260 CrossRef Medline
65. Lang, M. J., Martinez-Marquez, J. Y., Prosser, D. C., Ganser, L. R., Buelto, D., Wendland, B., and Duncan, M. C. (2014) Glucose starvation inhibits autophagy via vacuolar hydrolysis and induces plasma membrane internalization by down-regulating recycling. *J. Biol. Chem.* **289,** 16736–16747 CrossRef Medline
66. Kim, J., Lee, H. Y., Ahn, J., Hyun, M., Lee, I., Min, K. J., and You, Y. J. (2016) NHX-5, an endosomal Na^+/H^+ exchanger, is associated with metformin action. *J. Biol. Chem.* **291,** 18591–18599 CrossRef Medline
67. Onken, B., and Driscoll, M. (2010) Metformin induces a dietary restriction-like state and the oxidative stress response to extend *C. elegans* healthspan via AMPK, LKB1, and SKN-1. *PLoS One* **5,** e8758 CrossRef Medline
68. Roemer, T., and Krysan, D. J. (2014) Antifungal drug development: challenges, unmet clinical needs, and new approaches. *Cold Spring Harb. Perspect. Med.* **4,** a019703 CrossRef Medline
69. Gray, K. C., Palacios, D. S., Dailey, I., Endo, M. M., Uno, B. E., Wilcock, B. C., and Burke, M. D. (2012) Amphotericin primarily kills yeast by simply binding ergosterol. *Proc. Natl. Acad. Sci. U.S.A.* **109,** 2234–2239 CrossRef Medline
70. Rao, A., Zhang, Y., Muend, S., and Rao, R. (2010) Mechanism of antifungal activity of terpenoid phenols resembles calcium stress and inhibition of the TOR pathway. *Antimicrob. Agents Chemother.* **54,** 5062–5069 CrossRef Medline
71. da Silva, C. R., de Andrade Neto, J. B., Sidrim, J. J., Angelo, M. R., Magalhães, H. I., Cavalcanti, B. C., Brilhante, R. S., Macedo, D. S., de Moraes, M. O., Lobo, M. D., Grangeiro, T. B., and Nobre Júnior, H. V. (2013) Synergistic effects of amiodarone and fluconazole on Candida tropicalis resistant to fluconazole. *Antimicrob. Agents Chemother.* **57,** 1691–1700 CrossRef Medline
72. Mitterreiter, S., Page, R. M., Kamp, F., Hopson, J., Winkler, E., Ha, H. R., Hamid, R., Herms, J., Mayer, T. U., Nelson, D. J., Steiner, H., Stahl, T., Zeitschel, U., Rossner, S., Haass, C., and Lichtenthaler, S. F. (2010) Bepridil and amiodarone simultaneously target the Alzheimer's disease β- and γ-secretase via distinct mechanisms. *J. Neurosci.* **30,** 8974–8983 CrossRef Medline
73. Prasad, H., and Rao, R. (2015) Applying knowledge of autism to brain cancer management: what do we know? *Future Oncol.* **11,** 1847–1850 CrossRef Medline
74. Nixon, R. A. (2005) Endosome function and dysfunction in Alzheimer's disease and other neurodegenerative diseases. *Neurobiol. Aging* **26,** 373–382 CrossRef Medline
75. Prasad, H., Osei-Owusu, J., and Rao, R. (2017) Functional analysis of Na^+/H^+ exchanger 9 variants identified in patients with autism and epilepsy. *Matters* **2017** CrossRef Medline
76. Kondapalli, K. C., Llongueras, J. P., Capilla-González, V., Prasad, H., Hack, A., Smith, C., Guerrero-Cázares, H., Quiñones-Hinojosa, A., and Rao, R. (2015) A leak pathway for luminal protons in endosomes drives oncogenic signalling in glioblastoma. *Nat. Commun.* **6,** 6289 CrossRef Medline